ISOTOPE SYSTEMATICS OF THE EUCRITE JONZAC

A LOOK INTO THE HISTORY OF THE EUCRITE PARENT BODY USING THE

Lu-Hf, Sm-Nd, Pb-Pb, & U-Pb ISOTOPIC SYSTEMS

A Thesis Presented to

the Faculty of the Department of Earth & Atmospheric Science

University of Houston

In Partial Fulfillment

of the Requirements for the Degree

Master of Science

By

Jesse Evan Dietderich

December 2012

ISOTOPE SYSTEMATICS OF THE EUCRITE JONZAC

A LOOK INTO THE HISTORY OF THE EUCRITE PARENT BODY

USING THE Lu-Hf, Sm-Nd, Pb-Pb, & U-Pb ISOTOPIC SYSTEMS

_____

Jesse Evan Dietderich

APPROVED:

_____

Dr. Thomas J. Lapen

_____

Dr. Rasmus Andreasen

_____

Dr. Alan D. Brandon

_____

Dr. Kevin Righter

NASA Johnson Space Center

_____

Dr. Mark A. Smith, Dean, College of Natural Sciences and Mathematics

ACKNOWLEDGEMENTS

Only with the guidance of my committee members, help from my friends, and support from my family was I able to finish this master's thesis.

I would like to convey the deepest appreciation to my advisor, Tom, for his guidance, patience, and the opportunity to work on a research project such as this. I would like to thank Dr. Brandon, who was always there with witty banter and an intriguing perspective. I also need to thank Rasmus for all his assistance with the analyses on the multi collector, and his analytical knowledge that seemed as vast as the world's oceans. Furthermore, I must thank Dr. Righter, who was very generous each and every time that I journeyed down to NASA Johnson Space Center.

During numerous points of the analytical process Minako Righter was there to provide insight and support during the arduously long hours of lab period required during my thesis. I would have been lost during the laser ablation analysis without the help of Barry Shaulis, whom I deeply appreciate. I would like to thank Sam Simmons, who as a good friend, was always willing to give his expert opinion on lab protocol.

I would also like to thank my parents, Eric and Lisa, my best sister, Nicole, and my best friend, Amber Jean Tietgens. They were always encouraging me and supporting me with their best wishes.

Lastly, the venerable Cougar Grounds was able to keep me caffeinated when necessary, and the Flying Saucer kept me subdued during times of stress. Thanks to both, as their yin and yang kept me in balance through the entire endeavor.

ISOTOPE SYSTEMATICS OF THE EUCRITE JONZAC

A LOOK INTO THE HISTORY OF THE EUCRITE PARENT BODY USING THE Lu-Hf, Sm-Nd, Pb-Pb, & U-Pb ISOTOPIC SYSTEMS

An Abstract of a Thesis

Presented to

the Faculty of the Department of Earth & Atmospheric Science

University of Houston

In Partial Fulfillment

of the Requirements for the Degree

Master of Science

By

Jesse Evan Dietderich

December 2012

ABSTRACT

The main objective of this research is to understand the history of the eucrite parent body through the isotopic and petrologic study of the monomict eucrite Jonzac. Jonzac is a type 7 eucrite defined by less prominent Ca-zoning than that of type 4 eucrites and that it contains partly inverted pigeonite, which is a type 6 feature. The metamorphic textures observed include aggregates of polygonal pyroxene, jagged-shaped plagioclase, and recrystallization of the clastic matrix. Four isotopic systems (Lu-Hf, Sm-Nd, Pb-Pb, and U-Pb) were used to determine ages reflecting igneous formation and subsequent thermal and impact metamorphism of this meteorite. The igneous crystallization age is 4.546 ± 0.050 Ga (2σ) defined by U-Pb in zircon which we interpret as being the least prone to thermal disturbances. The other ages are either much younger or show signs of disturbances. A 4-point Lu-Hf isochron of age 4.236 ± 0.026 Ga (2σ; MSWD = 2.4) and a step-leaching 3-point Pb-Pb inverse isochron age of 4.352 ± 0.018 Ga (2σ; MSWD = 436) are much younger than the generally accepted formation interval for non-cumulate eucrites. A 4-point Sm-Nd isochron produced an 'age' of 4.733 ± 0.087 Ga (2σ; MSWD = 0.38). The discordant set of isochron ages indicate decoupling between isotope systems and support the hypothesis that the Lu-Hf, step-leaching Pb-Pb, and Sm-Nd isotope systems are disturbed. The ages likely reflect disturbances related to recrystallization during a period(s) of thermal metamorphism likely related to impact processes. The Lu-Hf and step leaching Pb-Pb ages place constraints on the timing of impact processes on the HED parent body and these ages are substantially older than the generally accepted period of late-heavy-bombardment (4.1 – 3.8 Ga) inferred from lunar studies.

Table of Contents

Appendices

List of Figures, Tables, & Equations

Figures

Tables

Equations

Chapter 1

Introduction

1.1 History of HED meteorites

The howardite-eucrite-diogenite (HED) series of achondrites were first grouped petrogenically by Mason (1967), and later by Clayton et al. (1976) and Clayton and Mayeda (1996) who used stable O isotopes to link them. Duke and Silver (1967) classified the eucrite group as either basalts or basaltic cumulates. While igneous orthopyroxenite cumulates were classified as diogenites (Mason, 1967), and mechanically combined clastic mixtures of both eucrites and diogenites were classified as howardites (McCarthy et al., 1972). Numerous observations point towards a single parent body source from which the HED meteorites originated. McCord et al. (1970) originally proposed that 4 Vesta was the source of these HED series meteorites, which has further been supported by two principal studies. One was based on similarities in reflection spectra between 4 Vesta and eucrites (Binzel and Xu, 1993). The other looked at small asteroids, called Vestoids, with similar orbital parameters and spectral similarities with Vesta, which are believed to have allowed the HED meteorites to obtain Earth-crossing orbits (Knezevic et al., 1991). With the help of the Hubble Space Telescope, there are more detailed surface observations that link that particular asteroid as the true HED

parent body (Binzel et al., 1997). Recently, NASA's Dawn mission has allowed further connections to be drawn between spectral analysis of Vesta's surface and laboratory spectra of HED meteorites samples (e.g. Reddy et al., 2012).

The monomict eucrite Jonzac was selected to be used to gain a greater understanding of the geologic and compositional history of the HED parent body. Jonzac was an observed fall on June 13th, 1819 in France's Poitou-Charentes region. The collected original mass was 5 kg, and has been subsequently split and shared with museum and academic institutions around the world. Studies have classified Jonzac even further as a monomict class eucrite. Monomict class eucrites, such as Stannern and Millibillillie, are commonly observed to have aggregates of polygonal pyroxene, jagged-shaped plagioclase, and a recrystallized clastic matrix (Yamaguchi et al., 1996). Particularly, Jonzac has a type 7 classification by Yamaguchi et al. (1996) due to the way that some low-Ca pyroxene grains are partially inverted, while at the same time having lower levels of Ca-zoning than other classification types. An explanation of the different classification types can be explained in Table 1. The slightly recrystallized clastic matrices of Jonzac have grains with smooth, curved grain boundaries, as well as larger fragments with their original angular shape. The selection of Jonzac was based on the classification as a non-cumulate eucrite, which allowed greater preservation of a uniform isotopic signature in the rock's mineral grains. Its recrystallized texture allows the investigation of the timing of thermal metamorphism and its relationship to the timing of impact processing on other solar system objects. Thus, Jonzac was an ideal choice for gaining further understandings of the HED parent body. According to previously

Table 1. Eucrite classification types. Types 1-6 details taken from Takeda and Graham, (1991), and type 7 details taken from Yamaguchi et al. (1996).

Type	Chemical zoning	Inversion to Opx	Clouding of pyroxene	Mesostasis glass	Exsolution of augite
1	fully preserved extensive zoning	none	none	preserved	TEM scale
2	metastable Fe-rich pyroxenes are absent	none	none	not clear	TEM scale
3	Fe-Ca trend from core to rim	none	trace	not clear	TEM scale coarsened
4	homogeneous host and remnant of zoning	none	present	recrystallized or absent	resolvable by EPMA
5	homogeneous host of exsolved pigeonite	stacking fault	present	recrystallized or absent	resolvable by EPMA
6	homogeneous host of exsolved pigeonite	partly inverted	present	recrystallized or absent	resolvable by EPMA
7	same as 4, less prominent Ca-zoning	partly inverted	present	recrystallized or absent	resolvable by EPMA

published chemical data, Jonzac lies on along the main group-Nuevo Laredo trend (see Figure 1). The previously published ages for Jonzac are limited to a U-Pb concordant age of 4.56 Ga (Bukovanska and Ireland, 1993), and a Pu-Xe age of 4.472 ± 0.016 Ga (Shukolyukov and Begemann, 1996).

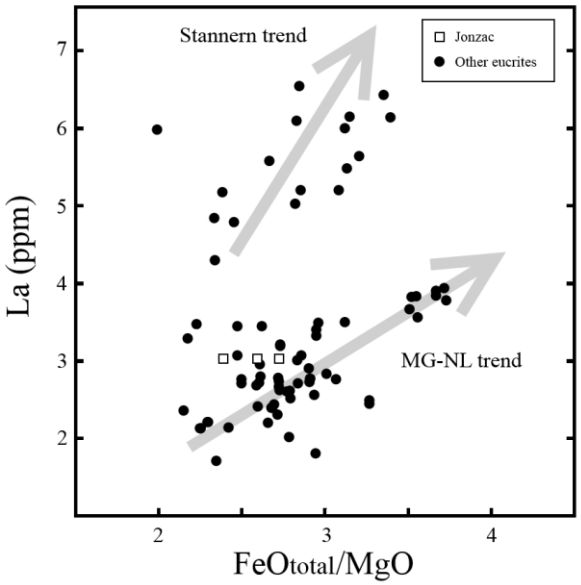

Figure 1. La vs. FeO_{total}/MgO plot for non-cumulate eucrites (falls and least weather finds). All three Jonzac points use La data from Barrat et al. (2000), while the FeO_{total}/MgO data are from Urey and Craig (1953), Barrat et al. (2000), and Stolper (1977). The other eucrite data are from original figure modified from Barrat et al. (2007) and references therein.

1.2 The Isotopic Systems

The elements Lu, Hf, Sm, and Nd are all refractory, making the Lu-Hf and Sm-Nd isotope systems ideal for understanding the chronology and silicate differentiation history of asteroids. Since these isotopic systems' parent and daughter nuclides are both lithophile and are fractionated by fractional crystallization/partial melting, they are sensitive to processes of crust-mantle differentiation. The Earth, Moon, and Mars are the three most studied planetary bodies, but all three have gone through various amounts of change since first accreting and differentiating. This can be contrasted by the relatively unmodified compositions of carbonaceous chondrites and ordinary chondrites which define the chondritic uniform reservoir (CHUR) (DePaolo and Wasserburg, 1976; Jacobsen and Wasserburg, 1980) for Lu-Hf and Sm-Nd. However, data in the literature (Bizzarro et al., 2003; Thrane et al., 2006) show that different initial $^{176}Hf/^{177}Hf$ isotopic values may exist for differentiated planetary and asteroidal bodies.

Previous studies of early solar system materials through the use of Pb-Pb analysis have proved to be fruitful (Amelin et al., 2002; Amelin, 2006; Amelin, 2008). The ability to leach out terrestrial Pb to allow for the meteoritic Pb to be detectable has yielded high-precision and accuracy ages of many varieties of meteorites, including eucrites. This vigorous method uses serial dissolution to peel away the layers of each mineral grain using progressively stronger acids until you are left with the most pristine Pb for extremely reliable meteoric data. U-Pb dating of zircons in eucrites (Bukovanska and Ireland, 1993; Misawa et al., 2005; Righter et al., 2011) allows for precise *in situ* dating of a sample while providing the earliest

crystallization age due to the high closure temperature for U-Pb in zircon (Cherniak et al., 1996).

Chapter 2

Objectives of Research

The objective of this research was to collect high-precision isotopic data of constituent minerals from the basaltic eucrite Jonzac. These data are used to construct internal isochrons that constrain crystallization ages and to determine the initial $^{176}Hf/^{177}Hf$ and $^{143}Nd/^{144}Nd$ isotope ratios for Jonzac. The age of Jonzac was expected to be acquired by high-precision Pb-Pb chronology using modified methods of Amelin (2008). This additional data would create an isochron that could be able to help determine the initial isotope compositions more accurately. Precision of the current techniques provide mineral formation dates within 0.5-1.0 Myr (Amelin, 2006).

Petrologic analysis of the sample provides a necessary context for the chronologic data. This work, conducted at the NASA Johnson Space Center, produced mineral maps and chemical analyses using their scanning electron microscope (SEM) and electron probe micro-analyzer (EPMA) instruments, respectively. Zircon was found during SEM imaging and was targeted for *in situ* analysis by laser ablation ICPMS to obtain U-Pb data that would define the igneous crystallization age for Jonzac.

Chapter 3

Analytical Methods

The Lu-Hf, Sm-Nd, and Pb-Pb isotopic data were obtained by a combination of column chemistry and mass spectrometry analysis for each element of interest. The U-Pb data were obtained by petrographic mapping and laser ablation analysis. The mineral chemical compositions were obtained by phase mapping and microprobe analysis. The following are an overview of the methods for preparing the samples for the mass spectrometers, how the mass spectrometers provided the data, how the data was converted into a usable form, and methods of error calculation.

3.1 Sample Selection/Preparation

The ~1 g-sized sample of the eucrite Jonzac was selected based on the non-cumulate nature. Also, the relatively unstudied isotopic systems of Jonzac were also expected to provide significant results to better understand the history of the HED parent body. Previous studies have never concentrated on as many different analyses of a class 7 eucrite.

Initial preparation began with the removal of fusion crust, followed by crushing and sieving a ~470 mg aliquot of sample into coarse-grain (100-200 mesh), fine-grain (200-325 mesh), and powder (>325 mesh) cuts. An untouched piece of Jonzac with the fusion crust removed was saved in order to make both thin and thick sections for

petrographic analysis. The crushing was achieved by using an alumina ceramic mortar and pestle, while the use of a Teflon sieve assisted in the sieving process. The coarse- and fine-grain cuts were then processed through a two-step heavy liquid separation. Acetylene tetrabromide was used first to separate out the plagioclase grains from the more dense phases. This was followed by thallium malonate processing in order to separate the pyroxene from the more dense oxide phases. The six cuts were then picked to ensure the purest mineral separates possible. Weights of each pure cut were recorded to ensure enough material was being dissolved for analysis. The purest fine-grain cuts of plagioclase and pyroxene were set aside for Pb chemistry, while the remaining cuts had the proper Sm-Nd and Lu-Hf spike amounts calculated based on the estimated amount of each element. These estimated amounts were calculated by averaging values of other known eucrites (Hsu and Crozaz, 1996). In order to achieve optimal spiking, a quantity of Lu-Hf mixed spike was added to the sample to bring the $^{178}Hf/^{177}Hf$ ratio to 2.2, and the $^{150}Nd/^{144}Nd$ ratio was brought to 0.5 with the Sm-Nd mixed spike. The fine-grained cut obtained from sieving was split and utilized to represent whole rock (WR) compositions. One of WR cuts was all powder, while the other incorporated the material picked out of all the pure cuts of plagioclase, pyroxene, and oxides into the remaining powder. The limited amount of pure oxide required the combination of both the coarse and fine-grain picked cuts to ensure measurable amounts of Lu. After the samples were carefully weighed, spikes were added to each of the cuts, and then the cuts were dissolved in Parr bombs in an 80/20 mixture of 2x distilled 29M HF and 2x distilled 14M HNO_3. The bombed samples were transferred into clean Savillex beakers and taken through repeated

evaporations with 2x distilled 14M HNO_3 to remove fluoride salts before chemical purification of the elements of interest.

The pure fine-grained plagioclase and pyroxene separates were weighed out into three aliquots. The two smaller aliquots of plagioclase and pyroxene were targeted for Pb-Pb dating and were taken through a leaching procedure that involved the following steps: 1) The sample was leached in 0.5 mL of 0.5M HNO_3 in an ultrasonic bath for 20 minutes. The acid was then pipetted in a clean beaker marked as Wash-1. The Wash-1 collection process was repeated an additional 3 times to ensure most surficial contamination was removed. 2) The next leaching step involved 0.5 mL of 6M HCl added to the sample, and the sample was then heated for 1 hour on a hotplate at 120 °C. The solution was then pipetted into a clean beaker marked as Wash-2. The Wash-2 collection process was repeated an additional 2 times with 6M HNO_3.

The larger aliquot of pyroxene was taken through a more vigorous serial dissolution process which included the same collection steps as the Wash-1 and Wash-2 described above, but with additional leaching steps. The full procedure for the leaching steps in addition to those listed above are as follows: 1) After Wash-2 was prepared from the sample aliquot, 1 mL of 6.0M HCl-0.2M HF was added to the sample, followed by 20 minutes in an ultrasonic bath, and then a 100 minutes of undisturbed rest on the lab counter at room temperature. The HCl-HF acid was then pipetted into a beaker labeled Wash-3, and the grains were rinsed 2 times with 1 mL of ~6M HCl, which was also pipetted in the Wash-3 beaker. 2) 1 mL of 6M HCl-2M HF was added to the sample, and then followed by 60 minutes on a hotplate at 120 °C. The HCl-HF acid was then pipetted

into a beaker labeled Wash-4, and the grains were rinsed twice with 1 mL of ~6M HCl, while pipetting these rinses in the Wash-4 beaker. 3) The final leaching step involved adding 1 mL of 7M HNO_3-14M HF, and then heating to 120 °C on a hotplate overnight. The HNO_3-HF acid was then pipetted into a beaker labeled Wash-5. Two rounds of 30 minute washes with 1 mL of ~6M HCl on a hotplate at 120 °C ensured dissolution of fluoride salts; these washes were also pipetted into the beaker labeled Wash-5. The remaining materials from the three aliquots and the wash solutions were then transferred to an ultra-clean set of mini Teflon capsules (for Pb use only) with 200 µL 29M HF and 50 µL 14M HNO_3, and were placed in a high-pressure digestion vessel heated to 150 °C for 48 hours to insure complete digestion. The goal of keeping Pb blank to a minimum was always paramount in any of the steps used to prepare the sample aliquots for analysis.

The small intact portion of Jonzac that was saved prior to crushing and sieving was sent to Johnson Space Center and mounted as a thin and thick section. The thick section, Jonzac-1, is 100 µm thick and has an average diameter of approximately 2.8 mm. The thin section, Jonzac-2, is 30 µm thick and has an average diameter of approximately 2.5 mm.

3.2 Column Chemistry

The Hf-Nd samples were processed through the first of four columns, where the cation resin held onto Fe allowing the remaining elements of interest to be passed through and collected. The second set of column chemistry used Ln-spec resin to allow for the

separation of Hf from my samples, while at the same time purifying the Hf cut by removing Ti and Zr (e.g. Münker et al., 2001). The Hf collected was then ready for analysis on the multi-collector ICPMS after transitioning it from HCl-HF over to HNO_3 phase. The major and rare earth element (REE) cut that was collected off the second column was then put through the third set of columns that incorporates Re-spec resin to help remove the remaining major elements and purify the REE even further. The fourth and final column used for the Hf-Nd samples utilized α-HIBA acid in order to separate out the REEs into Lu-Yb, Gd, Sm, and Nd cuts.

There was only one column used for Pb chemistry, but the samples were put through multiple rounds of Pb chemistry to ensure that the Pb was purified. Each sample was put through at least two rounds of chemistry before being considered for additional rounds. The 1.5 mL volume Pb columns used were hand-crafted using head shrink tubing, an aluminum plug machined to be the desired volume, the same frit material used in the glass columns, and a heat gun to bring it all together. The reason for creating small volume columns was to limit the amount of terrestrial Pb blank that would be introduced to the samples from the acids used in chemistry.

Initial concentration analysis of Pb on the multi-collector ICPMS made evident that the earlier washes had thallium contamination that was likely left over from the thallium malonate used during heavy liquid separation. This required a new method of thallium removal to be created for these Pb samples using the same columns used for cleaning the Pb samples. The most successful removal method mimicked the Pb purification chemistry, but the loading and eluting acids were remixed with 1% H_2O_2

added. The 1% H_2O_2 causes the thallium to stick to the resin by oxidizing it to Tl^{3+} while the Pb was allowed to elute with near 100% reclamation.

3.3 Hf Isotope Analysis

The Nu-Plasma II multi collector inductively coupled plasma mass spectrometer (MC-ICP-MS) at the University of Houston was used for analyzing the collected Lu and Hf cuts. During the first round of chemistry, the first picked oxide mineral separate was contaminated, which required a second picked oxide mineral separate to be prepared and run through chemistry. Due to sample contamination of the first oxide mineral separate, there were two runs for both Lu and Hf. The first runs for each element included all separates but the oxide cut (plagioclase, pyroxene, and whole rock separates), while the second run only had the oxide.

Prior to sample analysis on the MC-ICP-MS, concentration checks are done in order to determine the best method for running all samples at comparable concentration, and to make sure the standards that are being run in tandem have similar concentrations. To do this the dried down samples are brought up in 500 µL of 2% HNO_3 (or 2% HNO_3-1% HF when working with Hf). After allowing adequate time for sample to dissolve (heating on hotplate if needed), 10 µL is pipetted into an auto sampler vial containing 490 µL of 2% HNO_3 (or 2% HNO_3-1% HF when working with Hf). These 1:50 diluted samples were then analyzed to obtain concentration values, and the samples to be analyzed were diluted to be analyzed at 10 ppb, 25 ppb, or full concentration.

Hafnium samples and standards were introduced into the mass spectrometer via a micro-concentric desolvating nebulizer (Cetac Aridus II) in a 2% HNO_3-1% HF matrix at ~10-40 ppb concentration of Hf (samples were either 10 or 25 ppb, excluding the oxide that was run at full strength). Prior to introduction of sample, 60 seconds on-peak zero measurements were made using the same blank acid that was used during sample preparation. The nebulizer's uptake was ~120 µL/min, with each analysis consuming ~7.5 ng during the 6 minute run at 10 ppb. During analysis, the masses 173, 175, 181, and 182 (cups L4, L2, H4, and H5 respectively) were monitored in order to remove the ^{176}Lu and ^{176}Yb isobaric interferences on ^{176}Hf, ^{180}W + ^{180}Ta interference on ^{180}Hf, as well as ^{181}Ta interference on ^{181}Hf. The other masses monitored were 172, 174, 176, 177, 179, and 180 (cups L5, L3, L1, Ax, H1, H2, and H3 respectively). The isobaric interferences were corrected using the following isotopic compositions: ^{179}Hf/^{177}Hf = 0.7325, ^{176}Lu/^{175}Lu = 0.02656, ^{180}Ta/^{181}Ta = 0.000123, ^{176}Yb/^{172}Yb = 0.5845, and ^{180}W/^{182}W = 0.004521. To avoid any bias in 176 volts due the use of a mixed spike, the samples were underspiked for Lu, and the ^{176}Lu interference on ^{176}Hf was kept less than 0.005% via chemical purification. The instrumental mass fractionation on the isobaric interference correcting isotope ratios were compensated for by normalizing to ^{179}Hf/^{177}Hf = 0.7325 using an exponential law prior to adjustment of ^{176}Hf and ^{180}Hf volts. Between all analyses, not just Hf, on-peak zeros were taken to accurately subtract off total background the machine would have added to measurements. Unlike normal background subtractions, the on-peak zero method takes residual effects from previously run samples, and not just the background noise from the electronics. Instrumental mass bias and spike subtraction methods followed those in Lapen et al. (2004).

The $^{176}Hf/^{177}Hf$ operating values for the UW JMC-475 standard used during the first run analyses were; 25ppb = 0.282167 ± 0.000017 (2σ, n = 14), and 10ppb = 0.282157 ± 0.000002 (2σ, n = 2). The $^{176}Hf/^{177}Hf$ operating value for the PlasmaCal standard used during the first run analyses was 0.282159 ± 0.000016 (2σ, n = 14). The $^{176}Hf/^{177}Hf$ operating values for the in-house standards used during the first run analyses were; UH JMC-475 25ppb = 0.282196 ± 0.000013 (2σ, n = 59), UH JMC-475 10ppb = 0.282196 ± 0.000029 (2σ, n = 8), UH JMC-475 25ppb + Yb-Lu 6 ppt = 0.282205 ± 0.000014 (2σ, n = 10), UH AMES 25ppb = 0.282369 ± 0.000018 (2σ, n = 10), UH AMES 10ppb = 0.282350 ± 0.000006 (2σ, n = 2). For the second run for the oxide sample, $^{176}Hf/^{177}Hf$ operating values for the 10 ppb UW JMC-475 standard used during the analyses was 0.282143 ± 0.000033 (2σ, n = 4).

3.4 Lu Isotope Analysis

Lutetium isotope analysis is similar to the Hf analysis, except that Lu samples were brought up using a 2% HNO3 solution before being introduced into the MC-ICP-MS. The masses monitored during analysis were 171, 172, 173, 174, 175, 176, 177, 178, 179, 180, 181, and 182 (cups L5, L4, L3, L2, L1, Ax, H1, H2, H3, H4, H5, and H6 respectively). The masses 174, 176, and 180 were monitored in order to remove the ^{174}Hf isobaric interference on ^{174}Yb, the ^{176}Hf and ^{176}Yb isobaric interferences on ^{176}Lu, and the ^{180}W + ^{180}Ta interference on ^{180}Hf. Because it is difficult to separate Yb from Lu, we employed the isobaric interference and mass bias corrections for $^{175}Lu/^{176}Lu$ ratios of Vervoort et al. (2004).

3.5 Nd Isotope Analysis

Neodymium isotope analysis method is similar to the Lu method. The masses monitored during analysis were 140, 141, 142, 143, 144, 145, 146, 147, 148, 149, and 150 (cups L5, L4, L3, L2, L1, Ax, H1, H2, H3, H4, and H5 respectively). The masses 140 and 147 were monitored for ^{140}Ce and ^{147}Sm in order to calculate the isobar intensities of ^{142}Ce, ^{144}Sm, ^{148}Sm, and ^{150}Sm. These intensities were then used to remove the ^{142}Ce isobaric interference on ^{142}Nd, the ^{144}Sm isobaric interference on ^{144}Nd, the ^{148}Sm isobaric interference on ^{148}Nd, and the ^{150}Sm interference on ^{150}Nd. The isobaric interferences were corrected using the following isotopic compositions; ^{142}Ce/^{140}Ce = 0.7219, ^{144}Sm/^{147}Sm = 0.205023, ^{148}Sm/^{147}Sm = 0.749697, and ^{150}Sm/^{147}Sm = 0.4921. Instrumental mass bias and spike subtraction methods followed those in Lapen et al. (2004).

The ^{143}Nd/^{144}Nd operating values for the JNdi (Nu) standard used during the analyses were; 25ppb = 0.512105 ± 0.000010 (2σ, n = 7), and 10ppb = 0.512114 ± 0.000036 (2σ, n = 2). The ^{143}Nd/^{144}Nd operating values for the in-house standard, UH AMES, used during the analyses were; 25ppb = 0.511979 ± 0.000025 (2σ, n = 46) and 10ppb = 0.511979 ± 0.000018 (2σ, n = 2).

3.6 Sm Isotope Analysis

Samarium isotope analysis method is similar to the Lu and Nd methods. The masses monitored during analysis were 144, 145, 146, 147, 148, 149, 150, 151, 152, 153,

154, 155, and 156 (cups L5, L4, L3, L2, L1, Ax, H1, H2, H3, H4, H5, H6, and H7 respectively). Mass 146 and 155 were monitored for ^{146}Nd and ^{155}Gd in order to calculate the isobar intensities of ^{144}Nd, ^{148}Nd, ^{150}Nd, and ^{154}Gd. These intensities were then used to remove the ^{144}Nd isobaric interference on ^{144}Sm, the ^{148}Nd isobaric interference on ^{148}Sm, the ^{150}Nd isobaric interference on ^{150}Sm, the ^{152}Gd isobaric interference on ^{152}Sm, and the ^{154}Gd interference on ^{154}Sm. The isobaric interferences were corrected using the following isotopic compositions; ^{152}Gd/^{155}Gd = 0.013686, ^{154}Gd/^{155}Gd = 0.147335, ^{144}Nd/^{146}Nd = 1.38523, ^{148}Nd/^{146}Nd = 0.334642, ^{150}Nd/^{146}Nd = 0.327534, and ^{147}Sm/^{152}Sm = 0.560825.

3.7 Pb Isotope Analysis

The Triton Plus thermal ionization mass spectrometer (TIMS) at the University of Houston was used for running some of the collected Pb cuts. The first batch of Pb cuts were loaded onto rhenium filaments, coated with silica gel (to promote ionization) following methods of Gerstenburger and Haase (1997), mounted onto the turret, and placed in the TIMS. Only 50% of material from two samples in the first batch were saved for later analysis (12P40 Wash-2 and 12P42 Wash-2). The filaments were then heated up until a detectable Pb signal was able to be used to focus the beam with the use of charged plates in the source. The operating values for the 20 ng UH NBS-981 standards used during the TIMS analyses were; ^{206}Pb/^{204}Pb = 16.9195 ± 0.0135 (2σ, n = 4), ^{207}Pb/^{204}Pb = 15.4679 ± 0.0183 (2σ, n = 4), ^{208}Pb/^{204}Pb = 36.6249 ± 0.0554 (2σ, n = 4), ^{207}Pb/^{206}Pb = 0.914212 ± 0.000343 (2σ, n = 4), and ^{208}Pb/^{206}Pb = 2.16465 ± 0.00160 (2σ, n = 4). The

first batch of samples failed to yield usable data due to issues with ionization suppression from a suspected thallium (Tl) contamination.

The remaining samples from the first batch, along with the second batch of Pb cuts were then successfully run on the Nu-Plasma II multi collector inductively coupled plasma mass spectrometer (MC-ICP-MS) at the University of Houston. Samples were given initial concentration checks in the same way as the Hf-Nd samples. The concentration checks showed a Tl contamination issue for the early washes, and this would prevent accurate analysis until the Tl contamination was fully removed. After adequate Tl removal chemistry was done on all affected samples, the Pb samples were doped with 4 ppb of the UH NBS-997 Tl standard. This inclusion of Tl was to allow for correction of instrumental mass bias, because Pb has no stable isotope ratio which would allow for internal normalization.

Lead isotope analysis method is similar to the previous above methods. The masses monitored during analysis were 202, 203, 204, 205, 206, 207, 208, and 209 (cups L3, L2, L1, Ax, H1, H2, H3, and H4 respectively). Instrumental mass bias was corrected using the isotopic composition $^{205}Tl/^{203}Tl = 2.38890$ using the exponential mass bias law (Russell et al., 1978). The mass 202 was monitored for ^{202}Hg in order to calculate the isobar intensities of ^{204}Hg. These intensities were then used to remove the ^{204}Hg interference on ^{204}Pb. The isobaric interferences were corrected using the isotopic composition $^{204}Hg/^{202}Hg = 0.229866$.

Two Pb standards (UH NBS-981 and UH NBS-982) were doped with the UH NBS-997 thallium standard. The Pb operating values for 4 ppb of UH NBS-981 doped

with 4 ppb of UH NBS-997 were; $^{208}Pb/^{206}Pb$ = 2.1665 ± 0.0010 (2σ, n = 6), $^{207}Pb/^{206}Pb$ = 0.914629 ± 0.000203 (2σ, n = 6), $^{206}Pb/^{204}Pb$ = 16.9468 ± 0.0269 (2σ, n = 6), $^{207}Pb/^{204}Pb$ = 15.5003 ± 0.0271 (2σ, n = 6), and $^{208}Pb/^{204}Pb$ = 36.7165 ± 0.0753 (2σ, n = 6). While the Pb operating values for 2 ppb of UH NBS-982 doped with 4 ppb of UH NBS-997 were; $^{208}Pb/^{206}Pb$ = 1.000142 ± 0.000152 (2σ, n = 6), $^{207}Pb/^{206}Pb$ = 0.467044 ± 0.000093 (2σ, n = 6), $^{206}Pb/^{204}Pb$ = 36.8610 ± 0.1142 (2σ, n = 6), $^{207}Pb/^{204}Pb$ = 17.2153 ± 0.0567 (2σ, n = 6), and $^{208}Pb/^{204}Pb$ 36.8661 ± 0.1168 (2σ, n = 6). In the age calculations for the Pb-Pb inverse isochron, 2σ uncertainties were used.

3.8 Microprobe Analysis

The thick and thin section mounts (Jonzac-1 and Jonzac-2) were taken to Johnson Space Center (JSC) for analysis via EPMA in order to obtain chemical compositions of the mineral phases. Prior to microprobe analysis, both section mounts were carbon coated and then imaged using a SEM at 100x magnification. The SEM images were pieced together to make a complete map of each section mount. The main goal of the mapping was to find as many chromite grains as possible to allow for more detailed petrologic characterization, and secondarily, attempt to locate possible zircons.

After successfully locating and identifying nearly all heavy mineral phases in both sections, the sections were transferred to the Cameca SX-100 electron microprobe. The sets of JSC standards used for Jonzac were split between the oxide and silicate phases. The set of standards for the oxide phases are; Si [diopside], Al [chromite], Ti [rutile], Cr [chromite], V [V-metal], K [orthoclase-1], Zr [zirconia], Ca [diopside], Fe [chromite],

Mn [rhodonite], Hf [Sp-metal], Na [oligoclase], and Mg [chromite]. The set of standards for the silicate phases are; Si [diopside], Al [oligoclase], Ti [rutile], Cr [chromite], K [or1], Ca [diopside], Fe [fayalite], Mn [rhodonite], Na [oligoclase], and Mg [Marjalahti-olivine]. After calibrating the machine with standards, the mapped out grains were found and targeted for analysis. All zircon and chromite mineral grains were targeted, while the more abundant phases (ilmenite, high-, med-, and low-Ca pyroxene, plagioclase, silicate, troilite) selected throughout the sections in order to receive a fairly encompassing spread representing not a single area of the sections. Improperly identified phosphate phases during SEM mapping resulted in insufficient microprobe calibration to retrieve complete data for the phosphates.

3.9 U-Pb Isotope Analysis

The zircons found during SEM and microprobe work were small (1 μm – 10 μm), yet obtaining U-Pb data from these minerals is critical to this project. The quadrupole ICPMS at University of Houston was used to analyze all identified zircon grains in the thick section, Jonzac-1. Laser ablation analyses at the University of Houston were conducted with a Photon Machines Analyte.193 excimer laser with a 7.7 μm beam diameter at 7 Hz (140 total shots, 3 J/cm^2 fluence, He flow 0.550 L/min). Instrumental fractionation of U/Pb and $^{206}Pb/^{207}Pb$ during analyses was calibrated by analyzing fragments from zircon standard FC5z (1099 ± 1 Ma 2σ; Paces and Miller, 1993) and Plešovice (Sláma et al., 2008). All instrumental elemental and mass fractionation corrections and error propagation follow methods outlined in Shaulis et al. (2012).

Chapter 4

Results

The following tables contain the concentrations, isotopic ratios, and the errors associated with the measurements. Along with the isochron and concordia diagrams displaying how ages were obtained from the data. Chemical compositions of the constituent phases are also presented.

4.1 Calculated Dates

The Lu-Hf and Sm-Nd dates obtained were calculated based on the slope of the isochron and the y-intercept. Equation 1 was used for this calculation is;

$$T = \left(\frac{1}{\lambda}\right) \ln\left[1 + \frac{\left(\begin{matrix}daughter\\ratio\end{matrix}\right)_{sample} - \left(\begin{matrix}daughter\\ratio\end{matrix}\right)_{initial}}{\left(\begin{matrix}parent\\ratio\end{matrix}\right)_{sample} - \left(\begin{matrix}parent\\ratio\end{matrix}\right)_{initial}}\right] \quad \text{(Eq. 1)}$$

Where the time T is the calculated age, and λ is the decay constant for the parent isotope. The initial daughter ratio is the isochron's y-intercept value.

The date obtained from the Pb-Pb inverse isochron approach is based on a linear regression through $^{207}Pb/^{206}Pb$ and $^{204}Pb/^{206}Pb$ isotope ratio data. On an X-Y plot of $^{204}Pb/^{206}Pb$ and $^{207}Pb/^{206}Pb$ data, the Y-intercept of the linear regression through the data (the $^{207}Pb/^{206}Pb$ ratio at $^{204}Pb/^{206}Pb = 0$) indicates the radiogenic $^{207*}Pb/^{206*}Pb$ ratio

representing radiogenic ingrowth since the system was closed to Pb diffusion. A ^{207}Pb-^{206}Pb age is calculated from equation 2 using Isoplot v4.13 (Ludwig, 2003).

$$\left(\frac{^{207}Pb}{^{206}Pb}\right)^{*} = \frac{1}{137.88} \times \left[\frac{(e^{\lambda_{235}t}-1)}{(e^{\lambda_{238}t}-1)}\right] \quad \text{(Eq. 2)}$$

The U-Pb Concordia diagram is created by plugging a value for t into the following two equations (Equations 3 and 4) and generating coordinates that draw the curve on a ^{206*}Pb/^{238}U versus ^{207*}Pb/^{235}U diagram, otherwise known as a Concordia diagram. To get a concordant age from the diagram, you must have data that falls on top of Concordia curve. The closest point on the Concordia to the data point dictates the age.

$$\frac{^{206}\mathrm{Pb}*}{^{238}\mathrm{U}} = \frac{\left(\frac{^{206}\mathrm{Pb}}{^{204}\mathrm{Pb}}\right)_t - \left(\frac{^{206}\mathrm{Pb}}{^{204}\mathrm{Pb}}\right)_0}{\left(\frac{^{238}\mathrm{U}}{^{204}\mathrm{Pb}}\right)_t} = \mathrm{e}^{\lambda_{238}\mathrm{t}} - 1 \quad \text{(Eq. 3)}$$

$$\frac{^{207}\mathrm{Pb}*}{^{235}\mathrm{U}} = \frac{\left(\frac{^{207}\mathrm{Pb}}{^{204}\mathrm{Pb}}\right)_t - \left(\frac{^{207}\mathrm{Pb}}{^{204}\mathrm{Pb}}\right)_0}{\left(\frac{^{235}\mathrm{U}}{^{204}\mathrm{Pb}}\right)_t} = \mathrm{e}^{\lambda_{235}\mathrm{t}} - 1 \quad \text{(Eq. 4)}$$

4.2 Lutetium-Hafnium Results

The Lu and Hf isotope data for the plagioclase cut falls just off the isochron, similar to other studies (e.g. Shafer et al., 2010). The inclusion of the plagioclase has minimal effect on the age that the isochron provides (see Figure 1). From the data in

Table 2, a 4-point Lu-Hf isochron (excluding plagioclase) yielded an age of 4.236 ± 0.026 Ga, an initial $^{176}Hf/^{177}Hf$ value of 0.29932 ± 14 and MSWD = 2.4, Figure 2.

Table 2. Lu and Hf Data for Jonzac mineral separates. $^{176}Hf/^{177}Hf$ data is reported relative to JMC-475 = 0.282167 ± 0.000017 (2σ, n = 14). Uncertainties in the $^{176}Lu/^{177}Hf$ ratio are 0.2% based on the long-term reproducibility of replicate analyses of standards. All errors displayed as ± 2σ.

sample #	description	weight (g)	Lu (ppm)	Hf (ppm)	$^{176}Lu/^{177}Hf$	$^{176}Hf/^{177}Hf$
12HN8	Plagioclase	0.03267	0.0704	0.3740	0.02730	0.282242 ± 2
12HN9	Pyroxene	0.11999	0.3039	1.096	0.04020	0.283248 ± 2
12HN11	Whole Rock 1	0.03187	0.3450	1.255	0.02891	0.282314 ± 2
12HN12	Whole Rock 2	0.03013	0.2503	1.375	0.02484	0.281963 ± 2
12HN26	Oxide	0.00056	0.2357	16.51	0.00303	0.280186 ± 3

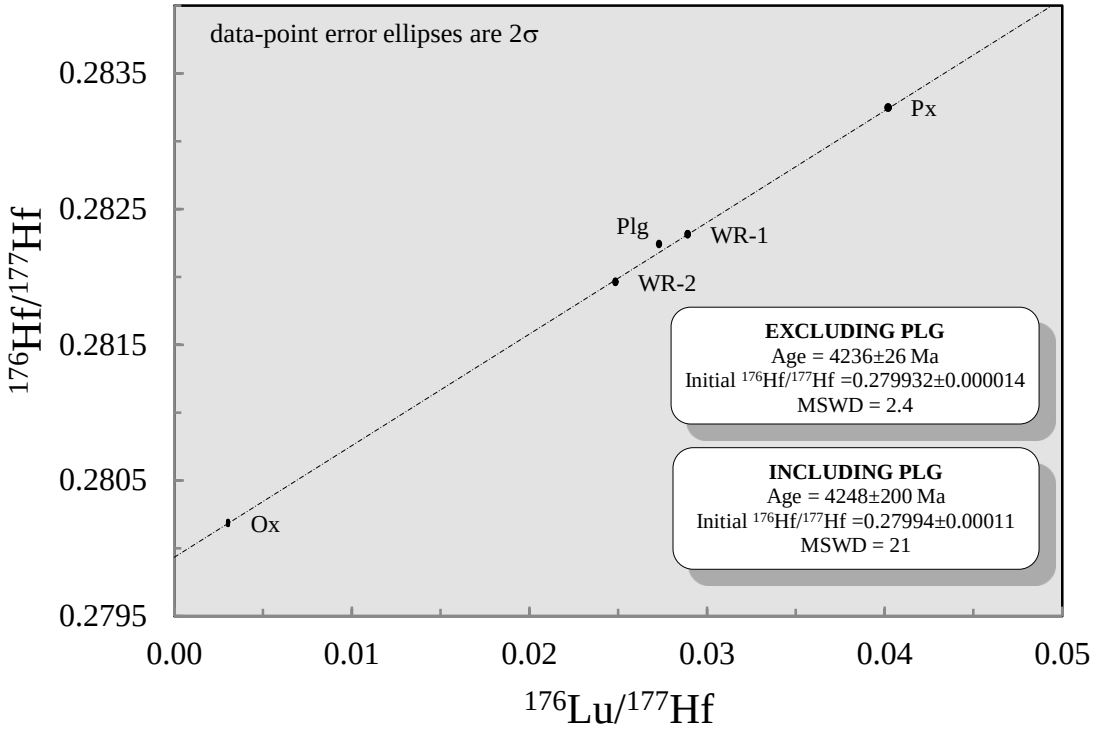

Figure 2. Lu-Hf isochron line excludes the plagioclase. The ages were obtained using a ^{176}Lu decay constant of $1.865x10^{-11}$ (Scherer et al., 2001). All errors displayed as ± 2σ.

4.3 Samarium-Neodymium Results

During the Sm and Nd oxide analysis, the oxide cut was unable to provide sufficient signal to be seen over background noise. This was expected due to the low amount of oxide dissolved and the pre-determined estimation of the oxide's Sm and Nd concentrations. Also, both the Sm and the Nd concentrations are half of what previously published concentration data shows for Jonzac (Barrat et al. 2000; Blichert-Toft et al. 2002). This would imply that the concentration of the University of Wisconsin mixed spike used was underestimated due to evaporation of the spike. The true higher concentration caused the reported Sm and Nd concentrations of Jonzac to be lower than they really are (see Table 3). From the data in Table 2, a 4-point Sm-Nd isochron yielded an age of 4.765 ± 0.088 Ga, an initial $^{134}Nd/^{144}Nd$ value of 0.50669 ± 11 and MSWD = 0.38, Figure 3. We have not yet ascertained the reason for the slope of the isochron that is too steep.

Table 3. Results from Sm and Nd samples analyzed on the multi-collector ICPMS. The Sm and Nd concentrations are not true concentrations, see above discussion for explanation. $^{143}Nd/^{144}Nd$ data is reported relative to JNdi (Nu) = 0.512105 ± 0.000010 (2σ, n = 7). Uncertainties in the $^{147}Sm/^{144}Nd$ ratio are 0.2% based on the long-term reproducibility of replicate analyses of standards. All errors displayed as ± 2σ.

sample #	description	weight (g)	Sm (ppm)	Nd (ppm)	$^{147}Sm/^{144}Nd$	$^{143}Nd/^{144}Nd$
12HN8	Plagioclase	0.03267	1.283	0.3710	0.1665	0.511952 ± 08
12HN9	Pyroxene	0.11999	2.304	0.8052	0.2013	0.513054 ± 11
12HN11	Whole Rock 1	0.03187	2.429	0.7951	0.1886	0.512655 ± 07
12HN12	Whole Rock 2	0.03013	2.624	0.8371	0.1837	0.512505 ± 09

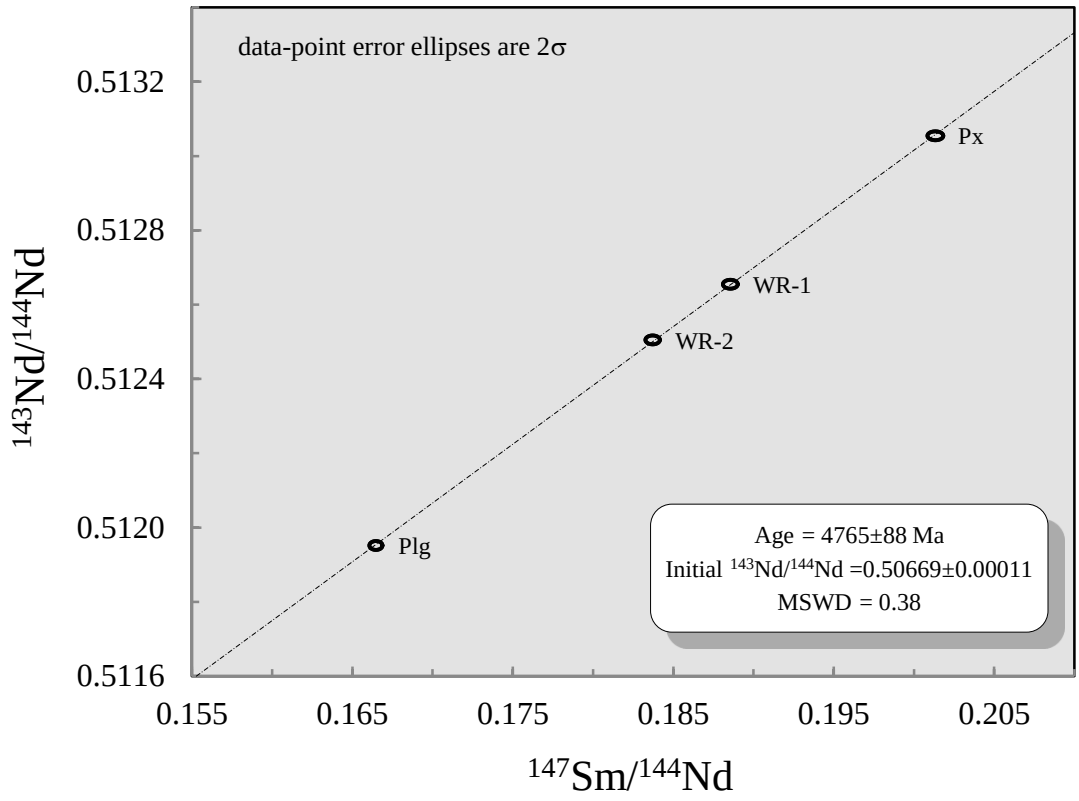

Figure 3. All obtained data are represented in this Sm-Nd isochron. The age was obtained using a ^{147}Sm decay constant of $6.539x10^{-12}$ (Scherer et al., 2001). All errors displayed as ± 2σ.

4.4 Lead-Lead Results

The first set of Pb samples run on the TIMS yielded no data, possibly due to suppressed ionization. The remaining samples from the first set (plagioclase wash-2 and pyroxene wash-2) were run on the multi-collector ICPMS, along with the second set of samples. Out of the four samples containing the most radiogenic Pb (pyroxene washes 2, 3, 4, and 5), the three with the greater intensities (pyroxene washes 2, 4, and 5), and thus lowest error, were used. From the data in Table 4, a 3-point Pb-Pb inverse isochron (excluding wash 3) yielded an age of 4.352 ± 0.018 Ga, an initial $^{207}Pb/^{206}Pb$ value of

0.5419 ± 0.0068 and MSWD = 436, Figure 4. The inclusion of wash-3 does not significantly alter the age. While constructing the inverse isochron, the sample with the largest overbearing amount of terrestrial Pb (pyroxene wash-1) wasn't included for being unable to identify a radiogenic Pb signature. On the other end, the lowest Pb intensity samples (plagioclase wash-2 and pyroxene residue) were also excluded from the isochron because of issues with detection limits causing large errors. The excluded data was plotted along with modern day Pb in Figure 5.

Table 4. Results for the successfully run Pb samples analyzed on the multi-collector ICPMS.
All errors displayed as ± 2σ.

sample #	description	$^{204}Pb/^{206}Pb$	$^{207}Pb/^{206}Pb$
12P40 W2	Plagioclase Wash-2	0.034984 ± 66	1.05048 ± 10
12P42 W1	Pyroxene Wash -1	0.055445 ± 09	0.86569 ± 03
12P42 W2	Pyroxene Wash -2	0.046834 ± 25	0.89787 ± 05
12P42 W3	Pyroxene Wash -3	0.007591 ± 31	0.60465 ± 05
12P42 W4	Pyroxene Wash -4	0.001056 ± 05	0.55045 ± 02
12P42 W5	Pyroxene Wash -5	0.003301 ± 11	0.56649 ± 02
12P42 Res	Pyroxene Residue	0.050602 ± 138	0.83127 ± 23

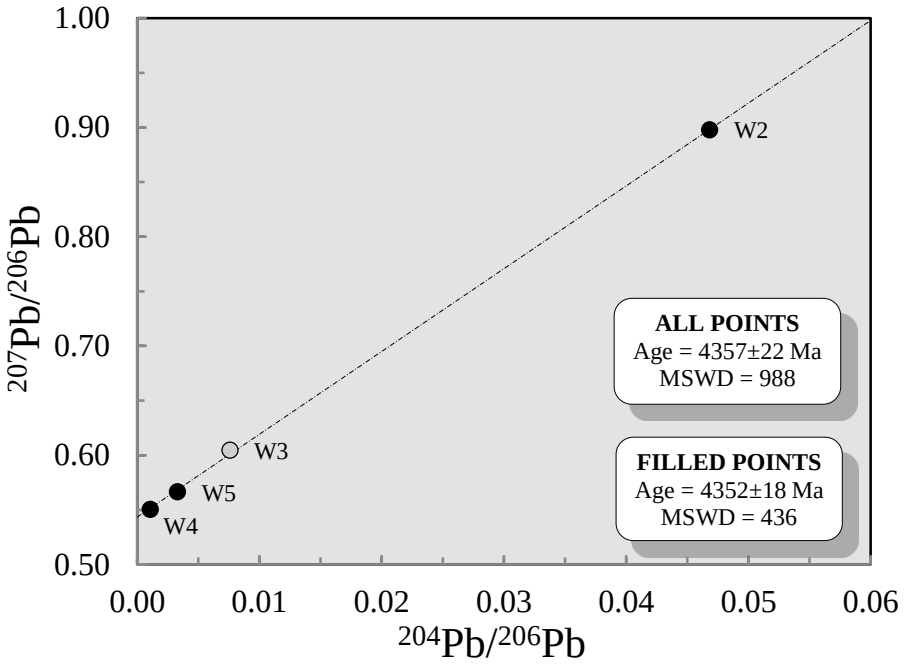

Figure 4. The Pb-Pb isochron line uses only pyroxene washes 2, 4, and 5. The ages were obtained using ^{235}U and ^{238}U decay constants of $9.8569x10^{-10}$ and $1.54993x10^{-10}$ (Schoene et al., 2006), respectively. All errors displayed as ± 2σ.

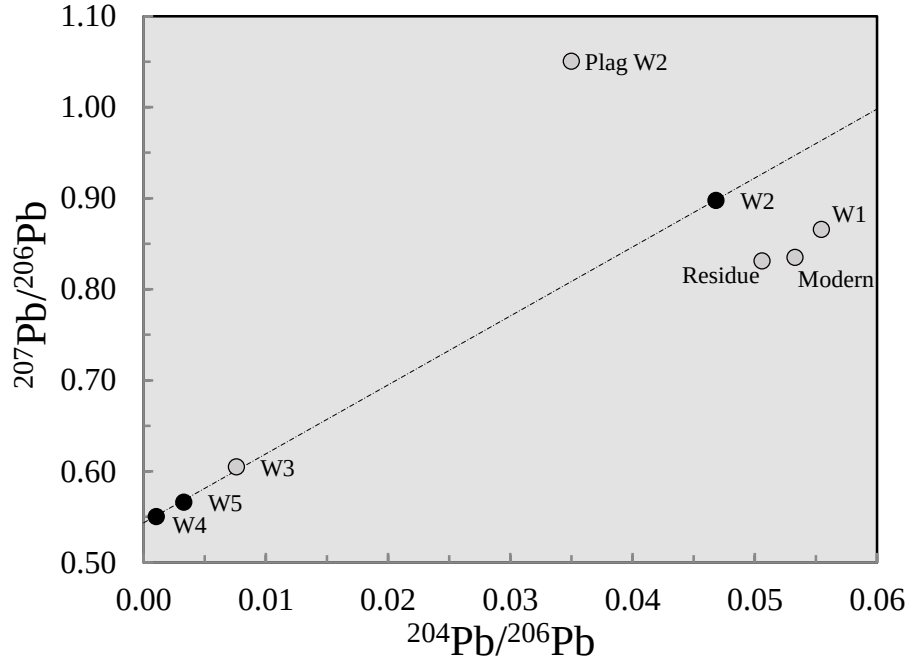

Figure 5. All Pb-Pb data plotted, in addition to modern day Pb values from Stacey and Kramers, (1975).

4.5 Uranium-Lead Results

The data collected by laser ablation were only from the largest of the zircon grains (Figure 6). The smaller grains were not able to provide a large enough integration window to produce reliable age dates. The FC5z standard is best because it yielded higher signals of ^{207}Pb than the younger Plešovice standard at 7.7 µm spot sizes resulting in a more robust correction of the unknown grains. From the FC5z corrected data in Table 5, a U-Pb concordia plot yielded an age of 4.546 ± 0.050 Ga, and MSWD = 0.12, Figure 7.

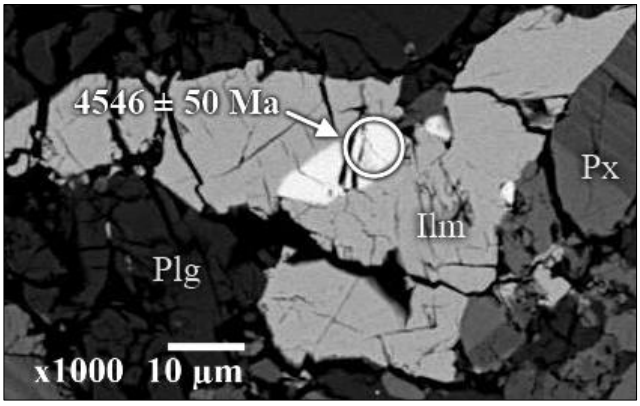

Figure 6. The back-scattered electron image of Jonzac-1, and the successful zircon analysis at 7.7 µm target spot size marked by the circle. The minerals surrounding the zircon include; ilmenite (Ilm), plagioclase (Plg), and pyroxene (Px).

Table 5. Zircon U-Pb data corrected using FC5z standard. The item 'rho' represents the correlation coefficient between the $^{207}Pb/^{235}U$ and $^{206}Pb/^{238}U$ isotope ratios. All errors displayed as ± 2σ.

$^{207}Pb/^{206}Pb$	$^{207}Pb/^{235}U$	$^{206}Pb/^{238}U$	rho	$^{208}Pb/^{238}U$ age	$^{207}Pb/^{235}U$ age	$^{207}Pb/^{206}Pb$ age	U ppm	Th ppm	U/Th
0.6221 ± 280	86.98 ± 4.70	1.014 ± 53	0.64	4513 ± 169	4546 ± 54	4560 ± 65	125	51	2.44

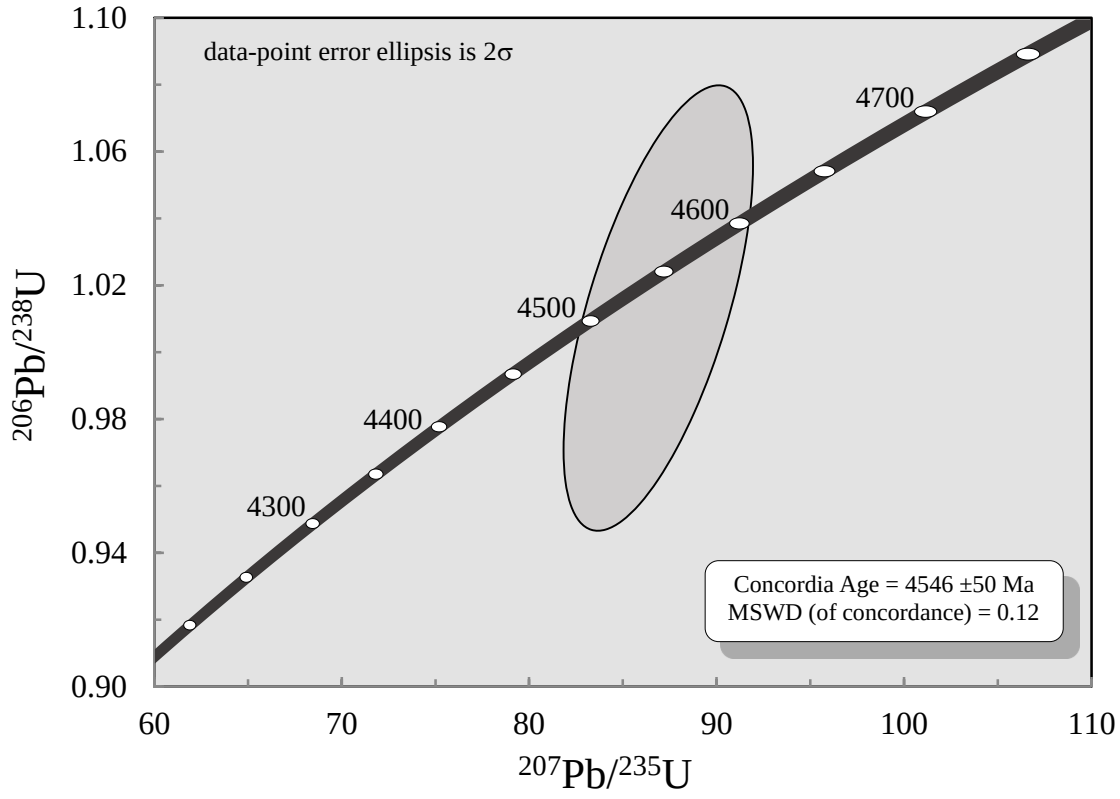

Figure 7. Concordia plot for zircon data corrected using the FC5z standard. The ages were obtained using ^{235}U and ^{238}U decay constants of 9.8569×10^{-10} and 1.54993×10^{-10} (Schoene et al., 2006), respectively. All errors displayed as ± 2σ.

4.6 Microprobe Data

The Jonzac pyroxene data obtained from the microprobe with averages for low-, med-, and high-Ca grains are listed in Table 6, along with previous published data for comparison. The entire dataset has been graphically displayed on a pyroxene quadrilateral (Figure 8) with other eucrites and diogenites. Jonzac's trend plots just between the Sioux County, a main-group eucrite, and Y-791195, a cumulate eucrite.

Table 6. Compositions of pyroxene grains from representative eucrites. Jonzac is from this study. The Jonzac low-Ca average is from 11 grains with analyses ranging from 1 to 8 per grain. The Jonzac med-Ca average is from 2 grains with analyses ranging from 2 to 3 per grain. The Jonzac high-Ca average is from 9 grains with analyses ranging from 1 to 10 per grain. Sioux County is a main group eucrite, Christophe Michel-Levy et al. (1987).

	Jonzac			Sioux County	
	low-Ca	med-Ca	high-Ca	low-Ca	high-Ca
			Chemical Composition (wt %)		
SiO_2	50.0	50.2	51.3	49.1	50.7
Al_2O_3	0.24	0.34	0.61	0.23	0.47
TiO_2	0.17	0.20	0.33	0.25	0.32
Cr_2O_3	0.16	0.12	0.24	0.42	0.39
FeO	35.7	31.8	17.2	36.1	16.6
MnO	1.17	1.04	0.58	1.12	0.53
MgO	12.2	11.9	10.6	11.7	9.84
CaO	1.00	5.29	19.3	0.78	20.8
Na_2O	nd	nd	0.03	nd	Nd
Total	100.63	100.87	100.21	99.70	99.65
			Cation Formula Based on 6 Oxygen		
Si	1.9871	1.9771	1.9756	1.9786	1.9695
Al	0.0113	0.0158	0.0277	0.0109	0.0215
Ti	0.0051	0.0061	0.0096	0.0076	0.0093
Cr	0.0051	0.0039	0.0072	0.0134	0.0120
Fe	1.1849	1.0484	0.5532	1.2166	0.5393
Mn	0.0393	0.0347	0.0190	0.0382	0.0174
Mg	0.7239	0.6976	0.6079	0.7027	0.5697
Ca	0.0425	0.2232	0.7957	0.0337	0.8658
Na	0.0006	0.0002	0.0026	--	--
Total Cations	3.9998	4.0070	3.9985	4.0017	4.0045
			*Cation Ratios Ca:Mg:Fe, Fe/Mn and mg# (100*Mg/(Mg+Fe))*		
Ca	2.2	11.3	40.7	1.7	43.8
Mg	37.1	35.4	31.1	36	28.8
Fe	60.7	53.2	28.3	62.3	27.3
Fe/Mn	30	30	29	32	31
mg#	37.9	40.0	52.4	36.6	51.4

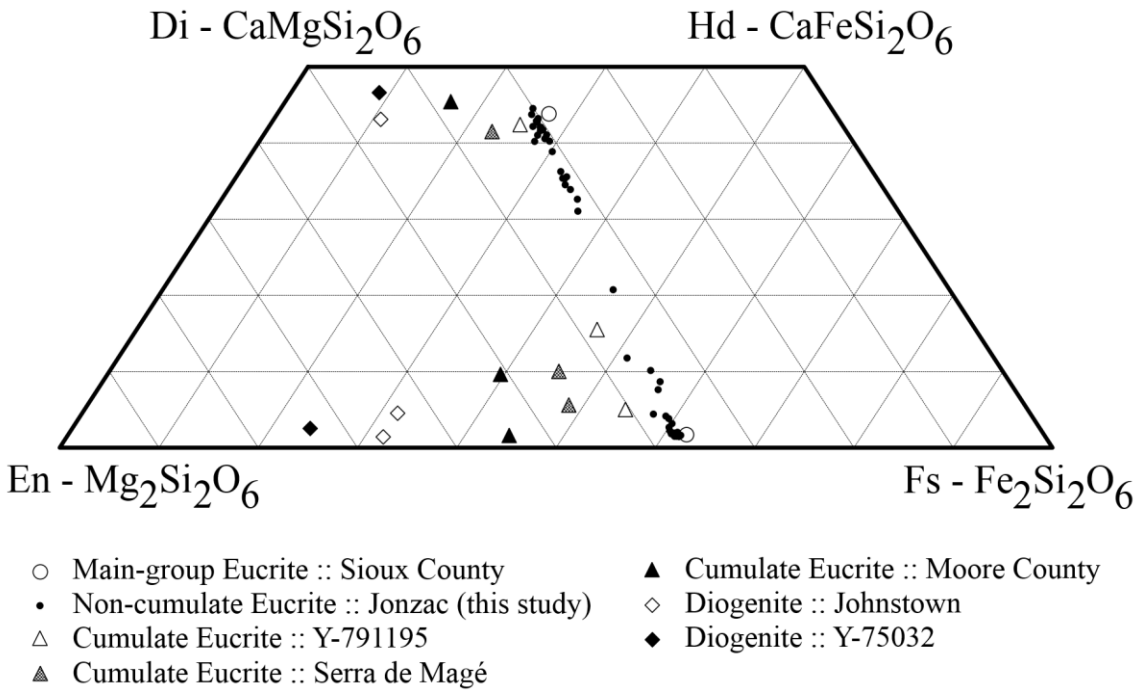

Figure 8. Pyroxene quadrilateral for pyroxenes found in eucrites and diogenites. The data for Sioux County, Christophe Michel-Levy et al. (1987); Jonzac, from this study; Y-791195, Mittlefehldt and Lindstrom (1993); Serra de Magé, Harlow et al. (1979); Moore County, Pun and Papike (1995); Johnstown, Fowler et al. 1994; Y-75032, Takeda and Mori (1985).

The low- and high-Ca pyroxene numbers were also used to calculate a closure temperature via two pyroxene thermometry equation (Equation 5) obtained from Brey and Kohler (1990). Where pressure (P) was set to 0 kbar, and elemental cation data was used to get T = 755 ± 81 °C.

$$T_{(K)} = \frac{23664+126.3\times\left(\frac{Fe}{Fe+Mg}\right)_{CPX}\times P}{13.38+\left[\ln\frac{(1-Ca/1-Na)_{CPX}}{(1-Ca/1-Na)_{OPX}}\right]^2+11.59\times\left(\frac{Fe}{Fe+Mg}\right)_{OPX}} \qquad \text{(Eq. 5)}$$

The Jonzac chromite and ilmenite data obtained from the microprobe are listed in Table 7, along with previous published data for comparison.

Table 7. Compositions of chromite and ilmenite grains from representative eucrites. Jonzac data is from this study. The Jonzac chromite average is from 9 grains with analyses ranging from 1 to 3 per grain. The Jonzac ilmenite average is from 7 grains with analyses ranging from 1 to 9 per grain. Sioux County is average chromite and ilmenite, main-group eucrite, Bunch and Keil (1971). Millbillillie is average chromite and ilmenite, main-group eucrite, Yamaguchi et al. (1994).

	Jonzac		Sioux County		Millbillillie	
	chromite	ilmenite	chromite	ilmenite	chromite	Ilmenite
			Chemical Composition (wt %)			
TiO_2	1.92	52.4	3.4	52.9	2.37	52.5
Al_2O_3	8.64	0.06	7.20	0.03	8.09	0.06
Cr_2O_3	51.9	0.09	51.6	0.06	52.6	0.03
V_2O_3	0.73	0.37	0.93	bd	nd	Nd
FeO	34.7	46.2	35.5	45.00	33.4	44.3
MgO	0.30	0.43	0.28	0.61	0.36	0.63
MnO	0.603	1.007	0.62	0.87	0.58	0.96
Total	98.78	100.55	99.53	99.47	97.40	98.48
			Cation Formula Based on 4 Oxygen			
Ti	0.0520	1.3144	0.0625	1.4013	0.0594	1.4107
Al	0.3658	0.0024	0.2074	0.0012	0.3177	0.0025
Cr	1.4752	0.0025	0.9970	0.0017	1.3856	0.0008
V	0.0209	0.0099	0.0182	--	--	--
Fe	1.0415	1.2903	0.7256	1.3256	0.9307	1.3237
Mg	0.0184	0.0285	0.0102	0.0320	0.0179	0.0335
Mn	0.0160	0.0215	0.0128	0.0260	0.0164	0.0291
Total Cations	2.9897	2.6694	2.0337	2.7878	2.7277	2.8003
			*Cation Ratios Cr:Al:2TI, Fe/Mn, mg# (100*Mg/(Mg+Fe)) and cr# (100*Cr/(Cr+Al))*			
Cr	75.9	-	75.0	-	76.0	-
Al	18.8	-	15.6	-	17.4	-
2Ti	5.3	-	9.4	-	6.5	-
Fe/Mn	65	60	57	51	57	46
mg#	1.7	1.6	1.4	2.4	1.9	2.5
cr#	80.1	50.5	82.8	57.3	81.3	25.1

The chromite dataset has been graphically displayed on a ternary plot (Figure 9) with other eucrites and diogenites. Jonzac's data plots with the other eucrite and diogenite data. The cumulate eucrites plot with the highest Ti values, the diogenites plot with the lowest values, and the main-group eucrites plot mostly in-between the other two. Unfortunately, Jonzac's data are fairly spread out, with the bulk of the data plotting on the low Ti end of the other main-group eucrites.

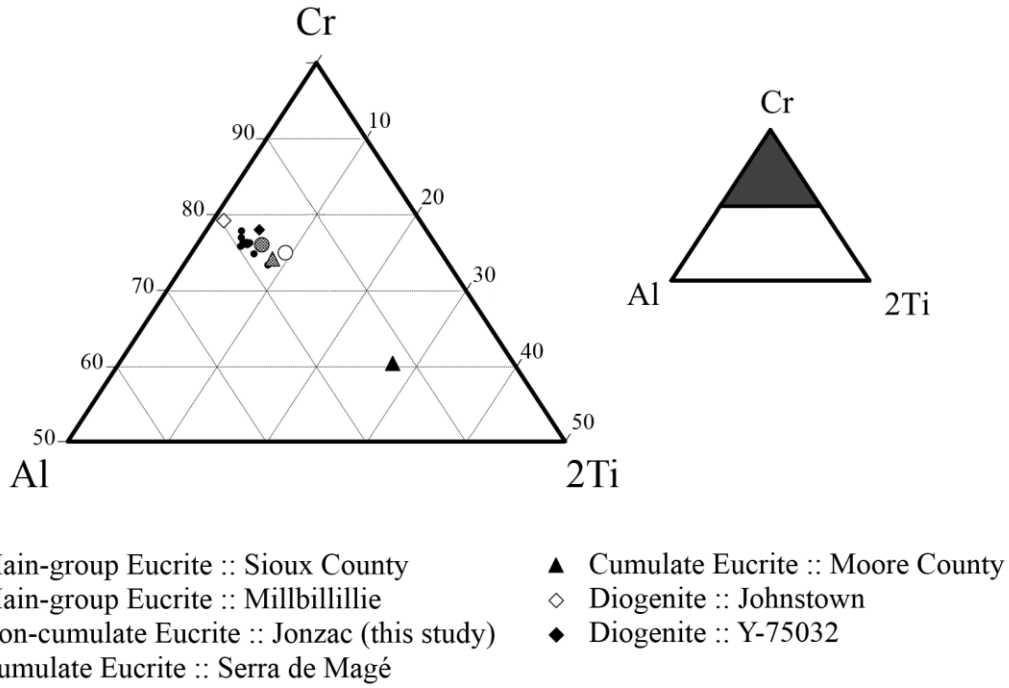

Figure 9. Ternary plot for chromite probe data for eucrites and diogenites. The figure to the left is a zoomed-in view of the figure to the right. The data for Sioux County, Christophe Michel-Levy et al. (1987); Millbillillie, Yamaguchi et al. (1994); Jonzac, from this study; Serra de Magé, Harlow et al. (1979); Moore County, Pun and Papike (1995); Johnstown, Fowler et al. 1994; Y-75032, Takeda and Mori (1985).

The Jonzac plagioclase data obtained from the microprobe are listed in Table 8, along with previous published main-group eucrite data for comparison.

Table 8. Plagioclase analyses for representative eucrites. Jonzac data is from this study. The Jonzac plagioclase average is from 8 grains with analyses ranging from 1 to 33 per grain. Juvinas and Pasamonte are average chromite and ilmenite, main-group eucrite, Bunch and Keil (1971).

	Jonzac	Juvinas	Pasamonte
	Chemical Composition (wt %)		
SiO_2	46.9	45.9	46.6
Al_2O_3	33.4	33.2	33
FeO	0.44	1.20	0.9
MgO	0.07	0.30	bd
CaO	17.2	18.0	17.4
Na_2O	1.55	1.00	1.8
K_2O	0.14	bd	bd
Total	99.66	99.60	99.70
	Cation Formula Based on 8 Oxygen		
Si	2.1643	2.1323	2.1588
Al	1.8160	1.8179	1.8020
Fe	0.0171	0.0466	0.0349
Mg	0.0049	0.0208	0.0000
Ca	0.8494	0.8960	0.8637
Na	0.1389	0.0901	0.1617
K	0.0084	0.0000	0.0000
Total Cations	4.9990	5.0037	5.0211
	*Cation Ratios mg# (100*Mg/(Mg+Fe)) and Molecular Proportion of Orthoclase (Or), Albite (Ab), Anorthite (An)*		
mg#	22	31	-
Or	0.8	-	-
Ab	13.9	9.1	15.8
An	85.2	90.9	84.2

The anorthite content of plagioclase in Jonzac (Figure 10) is consistent with other non-cumulate eucrites, and considerably lower than the cumulate eucrite data.

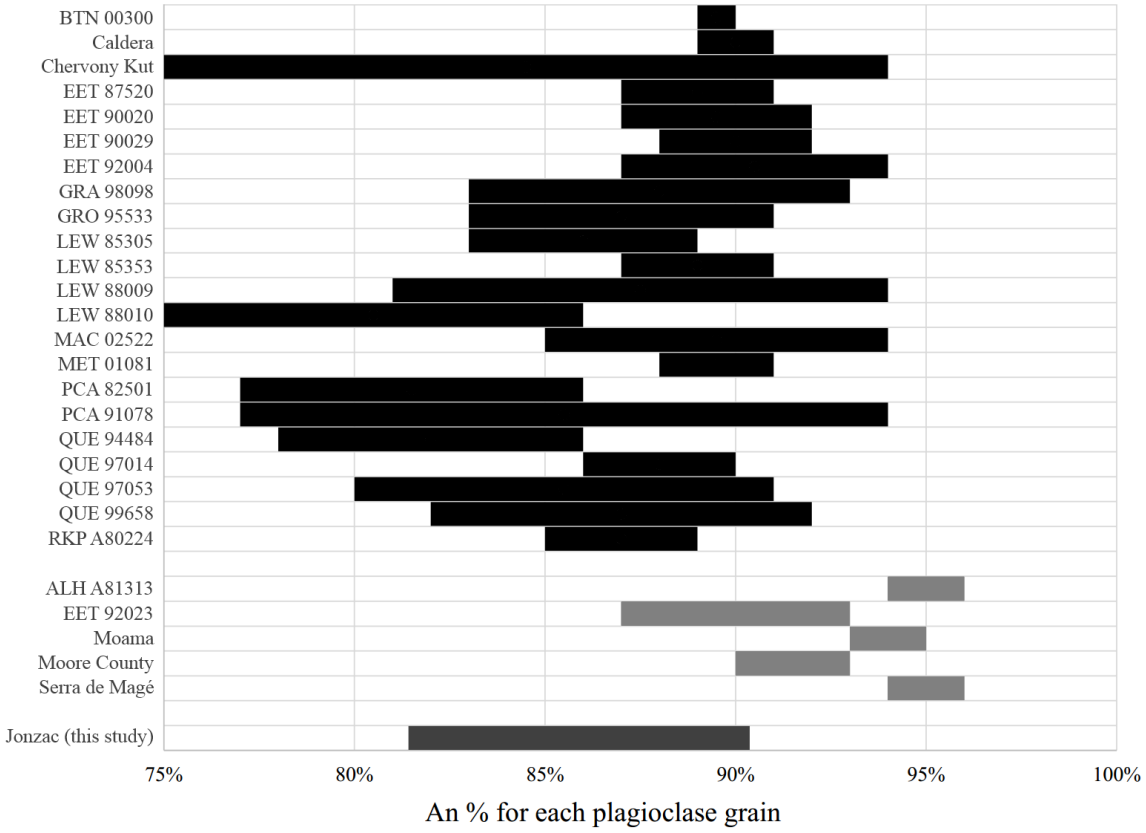

Figure 10. Anorthite (An) ranges for plagioclase analyses for eucrites. Black and light grey bars are basaltic and cumulate eucrite, respectively (modified from Mayne et al., 2009); Jonzac is the dark grey bar, from this study.

The Jonzac zircon data obtained from the microprobe are listed in Table 9, along with previous published monomict eucrite data for comparison. The zircon data differs mostly from the other monomict eucrites by having substantially more Fe and Ti, yet an unlisted sample, Y-75011, from Misawa et al., (2005) has similar compositions and was noted for having the electron beam spot overlapping surrounding ilmenite. The zircon

grains were small, measuring between 5 and 10 µm in diameter. At such small scales, the microprobe was having difficulty keeping the electron beam centered on the target grains. This drift caused much of the oxide data to be thrown out, and is a possible reason for the higher Fe and Ti values.

Table 9. Representative analysis of eucritic zircon (in wt %). Jonzac data is from this study. The Jonzac zircon average is from 2 grains with analyses ranging from 1 to 2 per grain. A-881388, A-881467, and Padvarninkai are monomict eucrites, Misawa et al. (2005).

	Jonzac	A-881388	A-881467	Padvarninkai
		Chemical Composition (wt %)		
SiO_2	31.8	32.4	32.5	33.0
Al_2O_3	0.01	0.00	0.01	0.01
TiO_2	1.7	0.00	0.16	0.03
FeO	1.9	0.66	0.34	0.78
MnO	0.02	0.03	0.01	0.01
MgO	0.001	0.02	0.02	0.02
CaO	0.06	0.12	0.02	0.11
Cr_2O_3	0.04	0.00	0	0.00
ZrO_2	63.895	66.0	66.3	64.7
HfO_2	1.565	0.96	1.31	1.42
Total	101.1	100.2	100.7	100.1

Chapter 5

Discussion

Here each isotopic system will be compared. The class 7 monomict eucrites are known to exhibit extensive recrystallization, yet no ages have yet to be published that match the ones determined for Jonzac in this study. The metamorphic textures and the implications for the thermal history of this stone will be discussed.

5.1 Age Comparisons

The 4-point 4.236 ± 0.026 Ga (2σ; MSWD = 2.4) Lu-Hf isochron age is over 200 million years younger than the inferred igneous crystallization interval for non-cumulate eucrites (e.g. Misawa et al., 2005). The 3-point Pb-Pb inverse isochron age of 4.352 ± 0.018 Ga (2σ; MSWD = 436) falls fairly close to the Lu-Hf age. These two young ages represent a resetting event that is much older than what would be expected from late heavy bombardment (Bogard and Garrison, 2009).

Table 10. Collection of age data from all explored systems. All errors displayed as ± 2σ.

System	mineral analysis	y-intercept	age
Lu-Hf Isochron	px-plag-WR-ox	0.279932 ± 14	4236 ± 26
Sm-Nd Isochron	px-plag-WR	0.50669 ± 11	4733 ± 87
Pb-Pb Inv. Isochron	px	0.5435 ± 84	4352 ± 18
U-Pb Concordia	zrc	-	4546 ± 50
U-Pb 207-206	zrc	-	4560 ± 65

The initial $^{143}Nd/^{144}Nd$ is far too low, and the 4-point Sm-Nd isochron age of 4.733 ± 0.087 Ga (2σ; MSWD = 0.38) is far too old to be a realistic age. When compared to literature data (see Figure 11), the $^{143}Nd/^{144}Nd$ ratio appears to plot within error, yet the $^{147}Sm/^{144}Nd$ has a significant spread that can only be attributed to a spiking problem. However, the same spike was used before and after on other projects and did not yield a similar anomaly in the reported data.

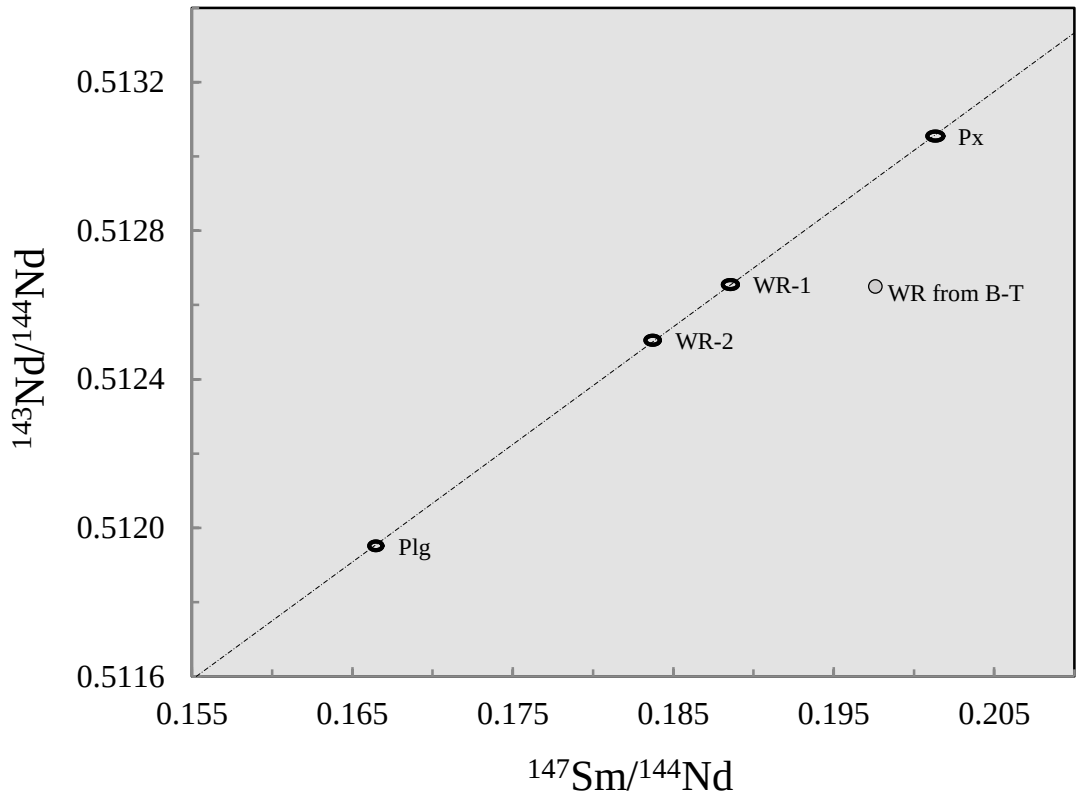

Figure 11. The data for Jonzac plotted against the published Sm-Nd whole rock data of Blichert-Toft et al. (2002).

The zircon ages measured by LA-ICPMS are 4.560 ± 0.065 Ga (2σ; ^{207}Pb-^{206}Pb) and a U-Pb concordia age of 4.546 ± 0.050 Ga (2σ) agree well with previously published zircon ages from eucrites (Misawa et al., 2005; Righter et al., 2011) as well as a previously analyzed zircon in Jonzac (concordant 4.56-Ga U-Pb; Bukovanska and

Ireland, 1993). These data allow us to confirm that the initial crystallization age of Jonzac is within the range of other zircon ages while the Lu-Hf and Pb-Pb isochrons ages reflect later disturbances likely due to thermal metamorphism.

5.2 Metamorphic/Thermal History

The igneous formation age of ~4.5 Ga for the eucrite parent body has been very well established with, for example, short-lived chronometers (e.g., Mn-Cr; Lugmair and Skukolyukov, 1998), by U-Pb zircon data (Bukovanska and Ireland, 1993; Misawa et al., 2005; Righter et al., 2011; this study), by coupled ^{142}Nd-^{143}Nd data (Andreasen and Sharma, 2006; Boyet et al., 2010), and by Pu-Xe (Shukolyukov and Begemann, 1996). The textures visible in SEM images (Figure 12) match those noted in Yamaguchi et al., (1996), which indicate brecciation and recrystallization. The relict grains of pyroxene that have gone through exsolution can be seen in Figure 12. While the highly disturbed/brecciated grain masses throughout the sample studied here (Figure 12). This indicates that Jonzac at one time has been part of events to have caused metamorphism to create the observed textures, and subsequently,

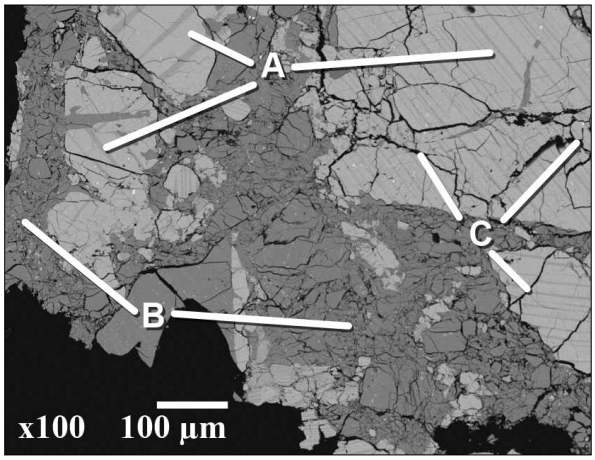

Figure 12. The back-scattered electron image of Jonzac. (A) Classic exsolution of pyroxene lamella in relict grains. (B) Disturbed/brecciated plagioclase grain mass. (C) Additional brecciation fractures of pyroxene.

additional events that caused further destruction and ultimately ejection from the parent body.

The Lu-Hf and Pb-Pb ages record such metamorphic disturbance at ages between ~4.2-4.3 Ga. The metamorphic processes that would have caused these systems to have reset would be situated between the initial igneous formation age, ~4.55 Ga, and the age in which the HED parent body was experiencing significant bombardment perhaps related to the late-heavy-bombardment (LHB; ~3.8-4.0 Ga; Bogard and Garrison, 2003). The data presented here suggests that the impact processes that resulted in metamorphism in Jonzac may have happened earlier than this interval. The study by Bogard and Garrison (2003) defended both the resilience of the Pu-Xe ages to thermal metamorphism, due to a greater resistance to degassing than the Ar-Ar system, and also the U-Pb/Pb-Pb ages where analyses of zircons are concerned. Other isotope systems such as Pb-Pb (non-zircon) and Sm-Nd provide ages where metamorphic disturbances are being recorded. Ar-Ar ages recorded for HED meteorites are often the youngest ages recorded, and can be attributed from impacting heating caused by bombardment.

According to Mayne et al. (2009), basaltic eucrites have exsolution temperatures between 654 and 1034 °C. The 2-pyroxene equilibration temperature data from this study, 755 ± 81 °C, fits within the expected range. Jonzac's temperature is on the low end, which may indicates a slow cooling rate. Slow cooling allows for exsolution lamella to be as abundant and thick as what is observed in Jonzac. The equilibration temperature data indicates subsolidus equilibration (Yamaguchi et al. 1996), and approach the equilibration temperatures observed in cumulate eucrites (e.g. Moore County, Takeda et

al. 1983). The Yamaguchi et al. (1996) study also indicated that type 7 eucrites could have experienced slower cooling and lower temperatures, as is evident by the remnant Ca-zoning.

This study's zircon data recording the igneous formation age is supported by the calculated closure temperature for Jonzac's zircon using the following equation from Dodson (1973).

$$T_c = R/[E \ln(A\tau D_0/\alpha^2)] \quad \text{(Eq. 6)}$$

Where R is the gas constant, E the activation energy, τ the time constant (calculated using the cooling rate), α takes into account the diffusion size, and A is a numerical constant dependent on the parent isotope.

A cooling rate of ~20 °C/Myr for Jonzac was inferred from the study of Haraiya by Schwartz and McCallum, (2005). Both Haraiya and Jonzac are type 7 eucrites, and as such, have similar cooling histories resulting in similar metamorphic textures. The resulting closure temperature for a 10 µm zircon was ~900 °C.

With an approximate temperature range inferred from Haraiya of ~1000 to 700 °C during a ~50,000 year thermal annealing period (Schwartz and McCallum, 2005), it can be concluded that the zircon used to obtain the Concordia age for this study would not have an affected U-Pb isotopic system. Jonzac did not spend enough time at temperatures above 900 °C.

Collected published isotopic ages of eucrites were turned into a histogram (see Figure 13) as a visual summation of the thermal history of all eucrites, including Jonzac. There is an apparent collection of formation ages around the 4.5-4.6 Ga, which is where all nearly all ages obtained from zircons plot. There is a seemingly lower abundance of Ar-Ar ages during the 4.1-4.4 Ga period, where Jonzac's thermally disturbed metamorphic ages (Pb-Pb and Lu-Hf) are plotted. Lastly, a long period of bombardment, as represented by the large span of Ar-Ar ages during the 3.4-4.0 Ga period.

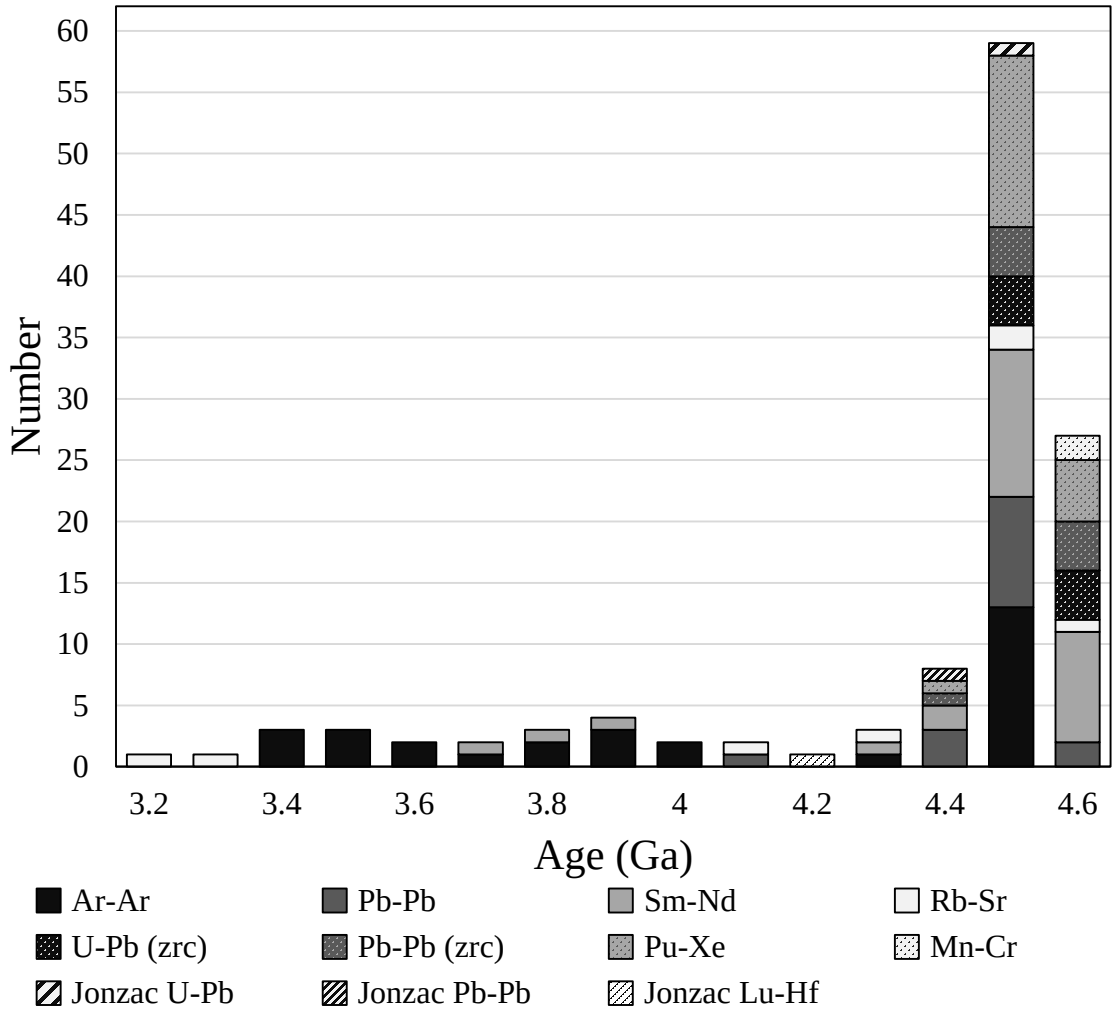

Figure 13. Histogram of eucrite age data rounded, including ages obtained in during this study. For a complete list of ages and sources used, refer to Appendix II.

CHAPTER 6

Conclusion

The precedence has already been established for the study of HED meteorites. Understanding 4-Vesta is easily within our grasp by using the same in-depth analysis which Jonzac experienced in this study. The potential to successful acquire five ages from multiple isotopic systems/methods, opens the door to what a single aliquot of sample can provide. It was hypothesized that this study would have yielded significant information about Jonzac, and that the additional petrographic research would provide new and useful data. To that extent, this study was a success.

The undisturbed igneous formation age provided by zircon analysis is supported by closure temperature data. The metamorphic disturbance of the Lu-Hf and Pb-Pb systems in Jonzac help place a lower boundary for continued thermal events not related to bombardment. Petrographic confirmation of type 7 attributes, and pyroxene exsolution thermometry help to provide a broader view of type 7 eucrites, such as Jonzac.

It is highly encouraged, that anyone looking into studying future meteoritic samples, to consider the complete gauntlet of dating and petrographic methods available, and to seek out further knowledge of other material from the HED parent body. Even with some methods failing to yield results (e.g. the Pb sample analyses on the TIMS), it

provided new methods to be developed (e.g. the Tl removal required for Pb sample analyses on the MC-ICP-MS). The end result of this study was not just a substantial data set for Jonzac, but a better set of tools to utilize for future studies.

References

Ahrens L.H., 1970. The composition of stony meteorites (VII) the special significance of eucrites Stannern and Nuevo Laredo in lunar-meteorite comparative studies. Earth and Planetary Science Letters, 9, 341-344.

Albarède F., Scherer E.E., Blichert-Toft J., Rosing M., Simionovici A., Bizzarro M., 2006. γ-ray irradiation in the Solar System and the conundrum of the ^{176}Lu decay constant. Geochem. Cosmochim. Acta., 70, 1261-1270.

Allègre C.J., Birck J.L., Fourcade S., Semet M.P., 1975. Rubidium-87/strontium-87 age of Juvinas basaltic achondrites and early igneous activity in the solar system. Science, 187, 436-438.

Amelin Y., Krot A.N., Hutcheon I.D., Ulyanov A.A., 2002. Pb isotopic ages of chondrules and Ca-Al rich inclusions. Science, 297, 1678-1683.

Amelin Y., 2006. The prospect of high-precision Pb isotopic dating of meteorites. Meteoritics and Planetary Science, 41(1), 7-17.

Amelin Y., 2008. U-Pb ages of angrites. Geochim. Cosmochim. Acta., 72, 221-232.

Andreasen R. and Sharma M., 2006. Solar nebula heterogeneity in p-process samarium and neodymium isotopes. Science, 314, 806-809.

Aylmer D., Herzog G.F., Klein J., Middleton R., 1988. ^{10}Be and ^{26}Al contents of eucrites: Implications for production rates and exposure ages. Geochim. Cosmochim. Acta., 52, 1691-1698.

Barrat J.A., Blichert-Toft J., Gillet Ph., Keller F., 2000. The differentiation of eucrites: The role of in situ crystallization. Meteoritics and Planetary Science, 35, 1087-1100.

Barrat J.A., Yamaguchi A., Greenwood R.C., Bohn M., Cotten J., Benoit M., Franchi I.A., 2007. The Stannern trend eucrites: Contamination of main group eucritic magmas by crustal partial melts. Geochim. Cosmochim. Acta., 71, 4108-4124.

Basaltic Volcanism Study Project, 1981. Basaltic volcanism on the terrestrial planets: The basaltic meteorites. Pergamon Press, Inc., New York., 214-235, 1286.

Binzel R.P. and Xu S., 1993. Chips off of asteroid 4 Vesta: Evidence for the parent body of basaltic achondrites meteorites. Science, 260, 186-191.

Binzel R.P., Gaffey M.J., Thomas P.C., Zellner B.H., Storrs A.D., Wells E.N., 1997. Geologic mapping of Vesta from 1994 Hubble Space Telescope images. Icarus, 128, 95-103.

Birck J.L. and Allègre C.J., 1978. Chronology and chemical history of the parent body of basaltic achondrites studied by the ^{87}Rb-^{87}Sr method. Earth and Planetary Science Letters, 39, 37-51.

Blichert-Toft J., Boyet M., Télouk P., Albarède F., 2002. ^{147}Sm-^{143}Nd and ^{176}Lu-^{176}Hf in eucrites and the differentiation of the HED parent body. Earth and Planetary Science Letters, 204, 167-181.

Bizzarro M., Baker J.A., Haack H., Ulfbeck D., Rosing M., 2003. Early history of Earth's crust-mantle system inferred from hafnium isotopes in chondrites. Nature, 421, 931.

Bogard D.D. and Garrison D.H., 2003. ^{39}Ar-^{40}Ar ages of eucrites and thermal history of asteroid 4 Vesta. Meteoritics and Planetary Science, 38(5), 669-710.

Bogard D.D. and Garrison D.H., 2009. Ar-Ar impact heating ages of eucrites and timing of the LHB. 40th Lunar Planetary Science Conference, abstract 1131.

Boyet M., Carlson R.W., Horan M., 2010. Old Sm-Nd ages for cumulate eucrites and redetermination of the solar system initial ^{146}Sm/^{144}Sm ratio. Earth and Planetary Science Letters, 291, 172-181.

Brey G.P. and Köhler T.K., 1990. Geothermobarometry in four-phase Lherzolites II. New thermobarometers, and practical assessment of existing thermobarometers. Journal of Petrology, 31(6), 1353-1378.

Bukovanská M. and Ireland T.R., 1993. Zircons in eucrites: Pristine and disturbed U-Pb systematics. Meteoritical Society, 28, 333.

Bunch T.E. and Keil K., 1971. Chromite and ilmenite in non-chondritic meteorites. Amer. Mineral, 56, 146-157.

Carlson R.W., Tera F., Boctor N.Z., 1988. Radiometric geochronology of eucrites Nuevo Laredo and Bereba. 19th Lunar Planetary Science Conference, 19, 166-167.

Cherniak D.J., Hanchar J.M., Watson E.B., 1996. Rare-earth diffusion in zircon. Chemical Geology, 134, 289-301.

Christophe Michel-Levy M., Bourot-Denise M., Palme H., Spettel B., Wänke H., 1987. L'eucrite de Bouvante: chimie, pétrologie et minéralogie. Bull Minéral, 110, 449-458.

Clayton R.N. and Mayeda T.K., 1996. Oxygen-isotope studies of achondrites. Geochim. Cosmochim. Acta., 60, 1999-2018.

Clayton R.N., Onuma N., Mayeda T.K., 1976. A classification of meteorites based on oxygen-isotopes. Earth and Planetary Science Letters, 30, 10-18.

Delaney J.S. and Prinz M., 1984. The polymict eucrites. 15th Lunar Planetary Science Conference, 15, 251-288.

DePaolo D.J. and Wasserburg G.J., 1976. Nd isotopic variations and petrogenetic models. Geophys. Res. Letts., 3, 249-252.

Dodson M.H., 1973. Closure temperature in cooling geochronological and petrological systems. Contr. Mineral. and Petrol., 40, 259-274.

Dreibus G., Spettel B., Wänke H., 1979. Halogens in meteorites and their primordial abundances. Physics and Chemistry of The Earth, 11, 33-38.

Duke M.B. and Silver L.T., 1967. Petrology of eucrites, howardites and mesosiderites. Geochim. Cosmochim. Acta., 31, 1637-1665.

Fowler G.W., Papike J.J., Spilde M.N., Shearer C.K., 1994. Diogenites as asteroidal cumulates: Insights from orthopyroxene major and minor element chemistry. Geochim. Cosmochim. Acta., 58, 3921-3929.

Gerstenberger H. and Haase G., 1997. A highly effective emitter substance for mass spectrometric Pb isotope ratio determinations. Chemical Geology, 136(3-4), 309-312.

Gibson E.K., Moore C.B., Primus T.M., Lewis C.F, 1985. Sulfur in achondritic meteorites. Meteoritics, 20(3), 503-511.

Harlow G.E., Nehru C.E., Prinz M., Taylor G.J., Keil K., 1979. Pyroxenes in Serra de Magé: Cooling history in comparison with Moama and Moore County. Earth and Planetary Science Letters, 43, 173-181.

Heymann D., Mazor E., Anders E., 1969. Ages of calcium-rich achondrites - I. Eucrites. Geochim. Cosmochim. Acta., 82, 1241-1268.

Hsu W. and Crozaz G., 1996. Mineral chemistry and the petrogenesis of eucrites: I. Noncumulate eucrites. Geochim. Cosmochim. Acta., 60(22), 4571-4591.

Jacobsen S.B. and Wasserburg G.J., 1980. Sm-Nd isotopic evolution of chondrites. Earth and Planetary Science Letters, 50(1), 139-155.

Jacobsen S.B. and Wasserburg G.J., 1984. Sm-Nd isotopic evolution of chondrites and achondrites, II. Earth and Planetary Science Letters, 67, 137-150.

Kaneoka I., 1981. ^{39}Ar-^{40}Ar ages of Antarctic meteorites Y-74191, Y-75258, Y-7308, Y-74450, and ALH 763. Proceedings of the 6th Symposium on Antarctic Meteorites, 20, 250-163.

Karpenko S.F., Smoliar M.I., Petaev M.I., Shukolyukov A., 1991. Rb-Sr and Sm-Nd systematics in Pomozdino meteorite. 16th Symposium on Antarctic Meteorites, 178-179.

Knezevic Z., Milani A., Farinella P., Froeschle Ch., Froeschle Cl., 1991 Secular resonances from 2 to 50 AU. Icarus, 93, 316-330.

Kumar A., Gopalan K., Bhandari N., 1999. 147Sm-143Nd and 87Rb-87Sr ages of eucrite Piplia Kalan. Geochim. Cosmochim. Acta., 63, 3997-4001.

Kunz J., Falter M., Jessberger E.K., 1997. Shocked meteorites: Argon-40 – argon-39 evidence for multiple impacts. Meteoritics and Planetary Science, 32, 647-670.

Lapen T.J., Mahlen N.J., Johnson C.M., Beard B.L., 2004. High precision Lu and Hf isotope analyses of both spiked and unspiked samples: A new approach. Geochem Cheophys Geosyst, 5, Q01010, doi: 10.1019/2003GC000582.

Ludwig K.R., 2003. Mathematical-statistical treatment of data and errors for Th-230/U geochronology. Uranium-Series Geochemistry, Reviews in Mineralogy and Geochemistry, 52, 631-656.

Lugmair G.W., 1974. Sm-Nd ages: a new dating method. Meteoritics, 9, 369.

Lugmair G.W. and Scheinin N.B., 1975. Sm-Nd systematics of the Stannern meteorite. Meteoritics, 10, 447-448.

Lugmair G.W., Scheinin N.B., Carlson R.W., 1977. Sm-Nd systematics of the Serra de de Magé eucrite. Meteoritics, 12, 300-301.

Lugmair G.W., Galer S.J.G., Carlson R.W., 1991. Isotope systematics of cumulate Eucrite EET-87520. Meteoritics, 26, 368.

Lugmair G.W. and Shukolyukov A., 1998. Early solar system timescales according to ^{53}Mn-^{53}Cr systematics. Geochim. Cosmochim. Acta., 62, 2863-2886.

Manhès G., Allègre C.J., Provost A., 1984. U-Th-Pb systematics of the eucrite "Juvinas": Precise age determination and evidence for exotic lead. Geochim. Cosmochim. Acta., 48, 2247-2264.

Mason B., 1967. The Bununu meteorite, and a discussion of the pyroxene-plagioclase achondrites. Geochim. Cosmochim. Acta., 31, 107-115.

Mayne R.G., McSween Jr. H.Y., McCoy T.J., Gale A., 2009. Petrology of the unbrecciated eucrites. Geochim. Cosmochim. Acta., 73, 794-819.

McCarthy T.S., Ahrens L.H., Erlank A.J., 1972. Further evidence in support of the mixing model for howardite origin. Earth and Planetary Science Letters, 15, 86-93.

McCord T.B., Adams J.B., Johnson T.V., 1970. Asteroid Vesta: Spectral reflectivity and compositional implications. Science, 168, 1445-1447.

Misawa K. and Yamaguchi A., 2001. U-Pb isotopic systematics of zircons from basaltic eucrites. Antarctic Meteorites, 26, 83-84.

Misawa K., Yamaguchi A., Kaiden H., 2005. U-Pb and ^{207}Pb-^{206}Pb ages of zircons from basaltic eucrites: Implications for early basaltic volcanism on the eucrite parent body. Geochim. Cosmochim. Acta., 69, 5847-5861.

Mittlefehldt D.W., 1986. Volatile degassing of basaltic achondrite parent bodies: Evidence from alkali elements and phosphorus. Geochim. Cosmochim. Acta., 51, 267-278.

Mittlefehldt D.W. and Lindstrom M.M., 1993. Geochemistry and petrology of a suite of ten Yamato HED meteorites. Proceedings of the NIPR Symposium on Antarctica Meteorites, 6, 268-292.

Miura Y.N., Nagao K., Sugiura N., Fujitani T., Warren P.H., 1998. Noble gases, ^{81}Kr-Kr exposure ages and ^{244}Pu-Xe ages of six eucrites, Béréba, Binda, Camel Donga, Juvinas, Millbillillie, and Stannern. Geochim. Cosmochim. Acta., 62(13), 2369-2387.

Münker C., Weyer S., Scherer E., Mezger K., 2001. Separation of high field strength elements (Nb, Ta, Zr, Hf) and Lu from rock samples for MC-ICPMS measurements. Geochemistry Geophysics Geosystems, 2(12), 1064-1082.

Nyquist L.E., Takeda H., Bansal B., Shih C.Y., Wiesmann H., Wooden J.L., 1986. Rb-Sr and Sm-Nd internal isochron ages of a subophitic basalt clast and a matrix sample from Y-75011 eucrite. Journal of Geophysical Research, 91, 8137-8150.

Nyquist L.E., Bogard D.D., Wiesmann H., Shih C.Y., Yamaguchi A., Takeda H., 1996. Early history of the Padvarninkai eucrite. Meteoritics and Planetary Science, 31, A101.

Nyquist L.E., Bogard D.D., Takeda H., Bansal B., Wiesmann H., and Shih C.Y., 1997. Crystallization, recrystallization and impact metamorphic ages of eucrites Y-792510 and Y-791186. Geochim. Cosmochim. Acta., 61, 2119-2138.

Nyquist L.E., Reese Y.D., Wiesmann H., Shih C.Y., Takeda H., 2001. Live ^{53}Mn and ^{26}Al in an unique cumulate eucrite with very calcic feldspar (An~98). Meteoritics and Planetary Science, 36, A151–152.

Nyquist L.E., Shih C.Y., Reese Y.D., 2008. Sm-Nd for norite 78236 and eucrite Y-980318/433: Implications for planetary and solar system processes. 39th Lunar Planetary Science Conference, abstract 1391.

Paces J.B. and Miller Jr. J.D., 1993. Precise U-Pb ages of Duluth Complex and related mafic intrusions, northeastern Minnesota: Geochronological insights to physical, petrogenetic, paleomagnetic, and tectonomagmatic processes associated with the 1.1 Ga Midcontinent Rift System. Journal of Geophysical Research, 98(B8), 13997.

Papanastassiou D.A., Wasserburg G.J., 1969. Initial strontium isotopic abundances and the resolution of small time differences in the formation of planetary objects. Earth and Planetary Science Letters, 5, 361-376.

Pun A. and Papike J.J., 1995. Ion microprobe investigation of exsolved pyroxene in cumulate eucrites: Determination of selected trace-element partition coefficients. Geochim. Cosmochim. Acta., 59, 2279-2289.

Quitté G., Birck J-L., Allègre C.J., 2000. ^{182}Hf-^{182}W systematics in eucrites: the puzzle of iron segregation in the early solar system. Earth and Planetary Science Letters, 184, 83-94.

Reddy V., Nathues A., Le Corre L., Sierks H., Li J., Gaskell R., McCoy T., Beck A.W., Schröder S.E., Pieters C.M., Becker K.J., Buratti B.J., Denevi B., Blewett D.T., Christensen U., Gaffey M.J., Gutierrez-Marques P., Hicks M., Keller H.U., Maue T., Mottola S., McFadden L.A., McSween H.Y., Mittlefehldt D., O'Brien D.P., Raymond C., Russell C., 2012. Color and albedo heterogeneity of Vesta from Dawn. Science, 336, 700-704.

Righter M., Lapen T.J., Shaulis B., 2011. U-Pb and ^{207}Pb-^{206}Pb age of zircons from basaltic eucrites. 42nd Lunar Planetary Science Conference, abstract 1608.

Righter M., Shaulis B., Lapen T.J., 2012. U-Pb and ^{207}Pb-^{206}Pb age of zircons from polymict eucrites and howardites. 43rd Lunar Planetary Science Conference, abstract 2562.

Russell W.A., Papanastassiou D.A., Tombrello T.A., 1978. Ca isotope fractionation on the Earth and other solar system materials. Geochim. Cosmochim. Acta., 42(8), 1075-1090.

Scherer E., Münker C., Mezger K., 2001. Calibration of the lutetium-hafnium clock. Science 293, 683-687.

Schoenberg R., Blanckenburg F., 2006. Modes of planetary-scale Fe isotope fractionation. Earth and Planetary Science Letters, 252, 342-359.

Schoene B., Crowley J.L., Condon D.J., Schmitz M.D., Bowring S.A., 2006. Reassessing the uranium decay constants for geochronology using ID-TIMS U-PB data. Geochim. Cosmochim. Acta., 70, 426-445.

Schwartz J.M. and McCallum I.S., 2005. Comparative study of equilibrated and unequilibrated eucrites; subsolidus thermal histories of Haraiya and Pasamonte. American Mineralogist, 90(11-12), 1971-1886

Shafer J.T., Brandon A.D., Lapen T.J., Righter M., Peslier A.H., Beard B.L., 2010. Trace element systematics and ^{147}Sm–^{143}Nd and ^{176}Lu–^{176}Hf ages of Larkman Nunatak 06319: Closed-system fractional crystallization of an enriched shergottite magma. Geochim. Cosmochim. Acta., 74, 7307-7328.

Shaulis B., Lapen T.J., Casey J.F., Reid D.R., 2012. Timing and rates of flysch sedimentation in the Stanley Group, Ouachita Mountains, Oklahoma and Arkansas, U.S.A.: Constraints from U-Pb zircon ages of subaqueous ash-flow tuffs. Journal of Sedimentary Research, (in press).

Shukolyukov A. and Begemann F., 1996. Pu-Xe dating of eucrites. Geochim. Cosmochim. Acta., 60(13), 2453-2471.

Sláma J., Košler J., Condon J.L., Gerdes A., Hanchar J.M., Horstwood M.S.A., Morris G.A., Nasdala L., Norberg N., Schaltegger U., Schoene B., Tubrett M.N., Whitehouse M.J., 2008. Plešovice zircon — A new natural reference material for U–Pb and Hf isotopic microanalysis. Chemical Geology, 249, 1-35.

Stacey J.S. and Kramers J.D., 1975. Approximation of terrestrial lead isotope evolution by a two-stage model. Earth and Planetary Science Letters, 26(2), 207-221.

Stolper E., 1977. Experimental petrology of eucritic meteorites. Geochim. Cosmochim. Acta., 41, 587-611.

Takeda H., Mori H., Delaney J.S., Prinz M., Harlow G.E., Ishii T., 1983. Mineralogical comparison of Antarctic and non-Antarctic HED (howardites-eucrites-diogenites) achondrites. National Institute of Polar Research, Memoirs, 30.D, 181-205.

Takeda H. and Mori H., 1985. The diogenite-eucrite links and the crystallization history of a crust of their parent body. Journal of Geophysical Research, 90, C636-C648.

Takeda H. and Graham A.L., 1991. Degree of equilibration of eucritic pyroxenes and thermal metamorphism of the earliest planetary crust. Meteoritics, 26, 129-134.

Takeda H., Mori H., Bogard D.D., 1994. Mineralogy and ^{39}Ar-^{40}Ar age of an old pristine basalt: Thermal history of the HED parent body. Earth and Planetary Science Letters, 122, 183-194.

Tatsumoto M., Knight R.J., and Allègre C.J., 1973. Time differences in the formation of meteorites as determined from the ratio of lead-207 to lead-206. Science, 180, 1279-1283.

Tatsumoto M., Unruh D.M., 1975. Formation and early brecciation of the Juvinas achondrite inferred from U-Th-Pb systematics. Meteoritics, 10, 500-501.

Tera F., Eugster O., Burnett D.S., Wasserburg G.J., 1970. Comparative study of Li, Na, K, Rb, Cs, Ca, Sr and Ba abundances in achondrites and in Apollo 11 lunar samples. Apollo 11 Lunar Science Conference, 2, 1637-1657.

Tera F., Carlson R.W., and Boctor N.Z., 1997. Radiometric ages of basaltic achondrites and their relation to the early solar system. Geochim. Cosmochim. Acta., 61, 1713-1731.

Thrane K., Bizzarro M., Baker J.A., 2006. Extremely brief formation interval for refractory inclusions and uniform distribution of ^{26}Al in the early solar system. Astrophysical Journal, 646, L159-L162.

Trinquier A., Birck J-L., Allègre C.J., Ulfbeck D., 2008. ^{53}Mn-^{53}Cr systematics of the early Solar System revisited. Geochim. Cosmochim. Acta., 72, 5146-5163.

Unruh D.M., Nakamura N., Tatsumoto M., 1977. History of the Pasamonte achondrite: relative susceptibility of the Sm-Nd, Rb-Sr and U-Pb systems to metamorphic events. Earth and Planetary Science Letters, 37, 1-12.

Urey H.C. and Craig H., 1953. The composition of the stone meteorites and the origin of the meteorites. Geochim. Cosmochim. Acta., 4, 36-82.

Vervoort J.D., Patchett P.J., Söderlund U., Baker M., 2004. Isotopic composition of Yb and the determination of Lu concentrations and Lu/Hf ratios by isotope dilution using MC-ICPMS. Geochemistry Geophysics Geosystems, 5, doi:10.1029/2004GC000721

Wadhwa M. and Lugmair G.W., 1995. Sm-Nd systematics of the eucrite Chervony Kut. Lunar Planetary Science, 26, 1453-1454.

Wadhwa M. and Lugmair G.W., 1996. Age of the eucrite Caldera from convergence of long-lived and short-lived chronometers. Geochim. Cosmochim. Acta., 60, 4889-4893.

Yamaguchi A., Takeda H., Bogard D.D., Garrison D., 1994. Textural variations and impact history of the Millbillillie eucrite. Meteoritics, 29, 237-245.

Yamaguchi A., Taylor G.J., Keil K., 1996. Global crustal metamorphism of the eucrite parent body. Icarus, 124, 97-112.

Yamaguchi A., Taylor G.J., Keil K., Floss C., Crozaz G., Nyquist L.E., Bogard D.D., Garrison D.H., Reese Y.D., Wiesmann H., Shih C.Y., 2001. Post-crystallization reheating and partial melting of eucrite EET90020 by impact into the hot crust of asteroid 4Vesta ~4.50 Ga ago. Geochim. Cosmochim. Acta., 65(20), 3577-3599.

Appendices

Appendix I – Previously Published Jonzac Data

Modal Mineral Abundances

all in (%)	Opx	Pig	Aug	Feld	Sili	Ilm	Cm	Phos	Troil
Delaney (1984)	25.8	16.2	10.8	44.7	1.5	0.5	0.3	0.1	0.2

Whole Rock Composition Data

all in (ppm)	Ba	Nd	Yb
Ahrens (1970)	26	5.36	1.56

all in (ppm)	Sc	Co	Ni	Cu	Zn	Ga	Rb	Sr	Y	Zr	Nb	Cs	Ba
Barrat et al. (2000)	29.9	8.5	1.5	8.6	6.3	1.58	0.64	74	17.27	39.01	3.27	0.020	30.4

La	Ce	Pr	Nd	Sm	Eu	Gd	Tb	Dy	Ho	Er	Yb	Lu
2.42	6.42	0.984	4.86	1.60	0.579	2.15	0.399	2.73	0.621	1.76	1.72	0.268

Hf	Ta	W	Th	U
1.05	0.183	0.049	0.313	0.092

all in (ppm)	K	^{87}Rb	^{86}Sr
Birck and Allegre (1978)	400	0.13	7.076

all in (ppm)	Lu	Hf	Sm	Nd
Blichert-Toft et al. (2002)	0.2628	1.264	1.666	5.098

all in (ppm)	F	Cl	Br	I
Dreibus et al. (1979)	15	5.1	0.021	0.01

in (ppm)	S
Gibson et al. (1985)	1180

Whole Rock Composition Data (continued)

all in (ppm)	Na	K	Rb	Cs
Mittlefehldt (1987)	3470	363	0.428	0.0147

all in (ppm)	Rb	Sr
Papanastassiou and Wasserburg (1969)	0.459	73.19

all in (ppm)	Hf	W
Quitte et al. (2000)	1.186	0.4028

	Li (ppm)	Na (%)	K (ppm)	Rb (ppm)	Cs (ppb)	Ca (%)	Sr (ppm)	Ba (ppm)
Tera et al. (1970)	9.65	0.332	329	0.405	13.9	7.16	74.6	29.0
duplicate	9.59	0.334	324	0.405	14.6	7.15	74.1	29.1
duplicate	9.43	-	327	0.404	14.6	-	74.2	29.3

all in (10^{-8} ccSTP/g)	He^3	He^4	Ne^{21}	Ar^{36}	Ar^{38}	Ar^{40}
Heymann et al. (1968)	37.1 ± 1.8	7300 ± 400	5.00 ± 0.25	3.82 ± 0.20	5.29 ± 0.27	2360 ± 120
duplicate	36.8 ± 1.8	9500 ± 500	4.94 ± 0.25	4.11 ± 0.20	5.67 ± 0.30	2780 ± 140

all in (ccSTP/g)	$^{136}Xe_{Pu}$	$^{126}Xe_{sp}$
Shukolyukov and Begemann (1996b)	3.27	2.29

all in (dpm/kg)	^{10}Be	^{26}Al
Aylmer et al. (1988)	25.8 ± 2.6	89.5 ± 1.4

all in (wt %)	SiO_2	TiO_2	Al_2O_3	Cr_2O_3	FeO	MnO	MgO	CaO	Na_2O	K_2O	P_2O_5
Barrat et al. (2000)	-	0.72	12.9	0.38	20.15	0.56	7.77	10.26	0.46	-	-
Stolper (1977)	49.3	0.73	12.6	0.25	18.2	0.47	6.7	10.2	0.61	-	-
Urey and Craig (1953)	48.32	0.52	12.73	0.33	17.76	0.28	7.42	10.48	0.91	0.22	0.16

Whole Rock Isotopic Ratios

	$^{176}Lu/^{177}Hf$	$^{176}Hf/^{177}Hf$ ($\pm 2\sigma/\sqrt{n}$)
Albarède et al. (2006)	0.0295	0.282404
Blichert-Toft et al. (2002)	0.02949	0.282404 ± 4

	$^{180}Hf/^{184}W \pm 2\sigma$	$^{182}W/^{184}W \pm 2\sigma$	εW
Quitte et al. (2000)	3.47 ± 0.03	0.864936 ± 24	2.2 ± 0.3

	$^{147}Sm/^{144}Nd$	$^{143}Nd/^{144}Nd$ ($\pm 2\sigma/\sqrt{n}$)
Blichert-Toft et al. (2002)	0.1976	0.512647 ± 13

	$^{87}Rb/^{86}Sr$	$^{87}Sr/^{86}Sr$
Birck and Allegre (1978)	0.01913	0.70016 ± 8
Papanastassiou and Wasserburg (1969)	0.01671	0.700062

	$\delta^{56}Fe \pm 2\sigma$	$\delta^{57}Fe \pm 2\sigma$	$\delta^{58}Fe \pm 2\sigma$
Schoenberg and von Blanckenburg (2006)	-0.016 ± 62	-0.002 ± 117	-0.05 ± 41

	$^{55}Mn/^{52}Cr$	$\varepsilon^{53}Cr$
Trinquier et al. (2008)	2.14	0.65 ± 0.10

Appendix II ─ Age List of Eucrites

Previous Published Eucrite Ages (U-Pb, Pb-Pb, Pu-Xe, and Mn-Cr)

Meteorite	Type	U-Pb	error	Pb-Pb	error	Pu-Xe	error	Mn-Cr	error	Source
A-881388	monomict	4.520	0.073							u
A-881467	monomict	4.565	0.01	4.551	0.014					t, u
				4.562	0.011					
Béréba	monomict	4.534	0.016	4.522	0.004	4.512	0.018			f, v, dd, hh
						4.498	0.016			
Bouvante	monomict			4.514	0.004	4.547	0.015			dd, hh
Cachari	monomict			4.453	0.015					hh
Caldera	unbrecciated			4.516	0.003					kk
Camel Donga	monomict					4.521	0.02			dd
Chervony Kut	monomict					4.538	0.019	4.5636	0.0009	r, dd
EET 79004	polymict	4.527	0.05	4.511	0.093					bb
EET 79006	polymict			4.446	0.25	(zircon)				cc
				4.523	0.12	(baddeleyite)				
EET 87520	cumulate			4.420	0.020					q
Jonzac	monomict					4.472	0.016			dd
Juvinas	monomict			4.539	0.004	4.548	0.023	4.5625	0.001	r, s, v, dd, gg
				4.556	0.012	4.551	0.015			
LEW 85300	polymict	4.450	0.024	4.486	0.037					cc
Millbillillie	monomict					4.522	0.016			v, dd
						4.507	0.021	(coarse-grain)		
						4.566	0.024	(fine-grain)		
Moama	cumulate			4.426	0.094					hh
Moore County	cumulate			4.484	0.019					hh
Nuevo Laredo	monomict			4.534	0.002	4.507	0.027			h, dd, hh
				4.514	0.015					
Padvarninkai	monomict	4.555	0.014	4.555	0.013	4.52	0.022			u, dd
Pasamonte	polymict			4.573	0.011	4.576	0.019			dd, ii
PCA 82502	unbrecciated					4.559	0.025			dd
Pomozdino	cumulate					4.559	0.015			dd
Serra de Magé	cumulate			4.399	0.035					hh
Sioux County	monomict			4.526	0.010	4.499	0.017			dd, ff
Stannern	monomict			4.128	0.016	4.434	0.013			v, dd, hh
						4.46	0.028			
Vetluga	monomict					4.479	0.022			dd
Y-75011	polymict	4.552	0.017	4.5501	0.0094					u
Y-792510	monomict	4.564	0.032	4.545	0.018					u

Previous Published Eucrite Ages (Ar-Ar, Sm-Nd, and Rb-Sr)

Meteorite	Type	Ar-Ar	error	Sm-Nd	error	Rb-Sr	error	Source
A-881388	monomict	4.480	0.007	4.54	0.15			c, z
A-881467	monomict			4.57	0.06			z
Béréba	monomict					4.08	0.26	g
Binda	cumulate			4.544	0.088			e
BTN 00300	unbrecciated	4.479	0.013					d
Caldera	unbrecciated	4.493	0.012	4.544	0.019			c, kk
Chervony Kut	monomict			4.55	0.03			jj
EET 87520	cumulate	4.473	0.011	4.547	0.009			c, q
EET 87548	cumulate	3.4	0.1					c
EET 90020	unbrecciated	4.486	0.008	4.43	0.03			c, q, y, ll
		4.489	0.013	4.51	0.04			
EET92023	unbrecciated	3.760	0.029					d
GRA 98098	unbrecciated	4.45	0.01					c
		4.49	0.02					
GRO 95533	unbrecciated	3.55	0.02					c
Juvinas	monomict			4.56	0.08	4.60	0.07	a, n
MET 01081	unbrecciated	3.715	0.054					d
Moama	cumulate	4.48	0.01	4.594	0.079			c, e, i
				4.46	0.03			
Moore County	cumulate	4.25	0.03	4.456	0.025			c, e, hh
				4.542	0.085			
Nagaria	cumulate	3.468	0.053					d
Padvarninkai	monomict	3.893	0.007	4.51	0.11			d, m, x
		3.88	0.01	3.71	0.01	(melt)		
				3.8	0.01	(basalt)		
Pasamonte	polymict			4.58	0.12			ii
PCA 82501	unbrecciated	3.778	0.016					d
PCA 92502	unbrecciated	4.506	0.009					c
Piplia Kalan	brecciated	3.5	0.1	4.57	0.023			c, l
Pomozdino	cumulate			4.54	0.12			k
QUE 97014	unbrecciated	3.54	0.03					c
QUE 97053	unbrecciated	4.480	0.015					c
Serra de Magé	cumulate	3.38	0.03	4.41	0.02			c, p
Stannern	monomict			4.48	0.07	3.2	0.5	b, o
Y-7308	unbrecciated	4.48	0.03					j
Y-75011	polymict	3.98	0.03	3.94	0.04	4.52	0.05	w, ee
				4.55	0.14	4.56	0.05	
Y-792510	monomict	3.4	0.16	4.34	0.06	4.26	0.62	y
		3.6	0.04	4.57	0.09	3.26	0.24	
Y-82202	monomict	3.925	0.006	(melt)				d
		3.950	0.026	(WR)				
Y-980318	cumulate			4.567	0.024			aa
Y-980433	cumulate			4.542	0.042			aa

Sources for Eucrite Ages

Please Note – errors reported above vary by publication

[a] Allègre et al. (1975)

[b] Birck and Allègre (1978)

[c] Bogard and Garrison (2003)

[d] Bogard and Garrison (2009)

[e] Boyet et al. (2010)

[f] Bukovanská and Ireland (1993)

[g] BVSP 1981

[h] Carlson et al. (1988)

[i] Jacobsen and Wasserburg (1984)

[j] Kaneoka (1981)

[k] Karpenko et al. (1991)

[l] Kumar et al. (1999)

[m] Kunz et al. (1997)

[n] Lugmair (1974)

[o] Lugmair and Scheinin (1975)

[p] Lugmair et al. (1977)

[q] Lugmair et al. (1991)

[r] Lugmair and Shukolyukov (1998)

[s] Manhès et al. (1984)

[t] Misawa and Yamaguchi (2001)

[u] Misawa et al. (2005)

[v] Miura et al. (1998)

[w] Nyquist et al. (1986)

[x] Nyquist et al. (1996)

[y] Nyquist et al. (1997)

[z] Nyquist et al. (2001)

[aa] Nyquist et al. (2008)

[bb] Righter et al. (2011)

[cc] Righter et al. (2012)

[dd] Shukolyukov and Begemann (1996)

[ee] Takeda et al. (1994)

[ff] Tatsumoto et al. (1973)

[gg] Tasumoto and Unruh (1975)

[hh]Tera et al. (1997)

[ii] Unruh et al. (1977)

[jj] Wadhwa and Lugmair (1995)

[kk] Wadhwa and Lugmair (1996)

[ll] Yamaguchi et al. (2001)